Static heavy quark-antiquark potential within string theory in arbitrary stationary backgrounds

Nikita Tsegelnik[*]
Joint Institute for Nuclear Research, Dubna 141980, Russia

(Received 16 February 2026; accepted 16 June 2026; published 16 July 2026)

We consider a static open string in arbitrary stationary spacetime, which can represent a heavy quark-antiquark pair within the holographic framework or effective theory. Generally, the string profile is not symmetric with respect to the turning point, and the symmetry restores for a simple string configuration in backgrounds with certain constraints. We identify a wide family of metrics for which the symmetry is preserved, enabling a direct isolation of the linear-in-distance term in the static potential for simple symmetric string configurations, even in nondiagonal backgrounds. As a first example, we apply our formulas to the black brane dual to the $\mathcal{N} = 4$ supersymmetric Yang-Mills (SYM) plasma at finite temperature. We find that the separation distance between quarks, L, is given in terms of a hypergeometric function, while the potential, V, consists of two distinct contributions: a term linear in the separation and a term that involves its derivative by temperature. Analysis of the leading terms in the series expansion reveals that the temperature corrections of the separation distance lead to the "swallowtail" behavior. Further, applying our formulas to the Rindler-anti–de Sitter (AdS) spacetime dual to an accelerated $\mathcal{N} = 4$ SYM plasma, we obtain analytic expressions for the distance and potential in terms of the elliptic integrals, which in the large Hawking temperature (large acceleration or small curvature) limit come to the conformal results for pure AdS. Then, we show that the distance between quarks decreases, the static potential between them increases, and the characteristic temperatures increase with an acceleration, a_c. However, we observe that an acceleration-scaled potential, $a_c V$, as a function of the acceleration-scaled distance, $a_c L$, does not depend on the certain value of the acceleration.

DOI: 10.1103/lhrn-rr2n

I. INTRODUCTION

Since the beginning of the 21st century, there has been active research into quantum field theory (QFT) in the presence of external fields or under extreme conditions. Such conditions—extreme temperatures, densities, rotation, acceleration, background electromagnetic fields or condensates—can fundamentally alter the theory dynamics. They may affect phase transitions, stabilize or destabilize various topological structures, or give rise to entirely new novel phenomena. These studies are crucial not only from a theoretical standpoint but also for interpreting modern high-energy experiments, where such extreme states are routinely created.

A prominent example is the physics of heavy-ion collisions (HIC), where generated electromagnetic fields are among the strongest in the known Universe. It has been predicted that the magnetic fields reaching up to 10^{18} Gauss may arise in noncentral collisions [1–9]. Such fields can significantly modify the quantum chromodynamics (QCD) behavior, catalyzing the deconfinement and chiral transitions via the inverse magnetic catalysis [10–16], inducing anomalous transport within the chiral magnetic effect [17–20], and generating the spin polarization [21–26]. Recently, a possibility of relatively long-lived strong electric fields has also been explored [27], offering a direct probe of nonperturbative vacuum decay and pair production via the Schwinger mechanism [28–30].

Another rapidly growing direction involves noninertial effects in QFT, which have gained considerable community interest following the observation of global spin polarization in HIC [31–34]. Contrary to early naive expectations of zero averaged polarization [35] and first controversial experimental evidences [36,37], these observations have spurred a comprehensive reexamination of the spin theory [21,38–47], establishing the thermal vorticity [39,48,49], consisting of rotation, acceleration, and temperature gradients, as the dominant source of the observed polarization signal in HIC.

With the large angular momentum of the initial system, huge pressure and temperature gradients lead to the

[*]Contact author: tsegelnik@theor.jinr.ru

generation of the vorticity [50–54]. Detailed modeling of the velocity and vorticity fields [39,48,49,52,54–61] indicates that the medium created in heavy-ion collisions exhibits extreme local rotation $\omega \sim 10^{21}$–10^{23} sec^{-1} and undergoes rapid collective expansion, whose early-time Hubble parameter exceeds the cosmological value by roughly 40 orders of magnitude. Notable, these predictions of the extreme values of the vorticity lead to the statement that quark-gluon plasma (QGP) is the fastest-rotating fluid in nature [32,62]. Recently, it was also shown that acceleration of the nuclear medium may reach extremely high values of $a \sim 0.1$–1 GeV [63].

All of these extreme kinematic conditions motivate wide theoretical studies of QFT in rotating [64–86] and accelerated [87–104] medium. It is also essential to note combined researches including rotation and electromagnetic fields [105–110]. Notably, recent lattice QCD calculations reveal striking results: the deconfinement (or chiral restoration) critical temperature exhibits opposite responses to rotation in the gluonic and fermionic sectors [111–116], negative moment of inertia and rotational instability of QGP [117–123].

These extreme conditions—strong external fields, rotation, acceleration, and high temperature/density—often correspond to strongly coupled regimes where traditional perturbative QCD methods fail. This strongly motivates the use of nontraditional methods, such as gauge/gravity duality, particularly the anti-de Sitter/conformal field theory (AdS/CFT) correspondence [124], as a powerful nonperturbative tool [125–127]. By mapping a gauge theory in $D-1$ dimensions to a classical gravitational theory in D-dimensional AdS space, holography provides geometric insight into a strongly coupled regime of the gauge theory.

In particular, the holography framework is successfully used in application to the calculations of the potential energy of the static quark-antiquark pair [128–138], studies of the confinement and deconfinement phases [139–150], evaluations of the radiative energy losses [151–156], and other problems [157–179]. There are also a lot of research in the presence of the electromagnetic fields (finite chemical potential and baryon density) [180–190], rotation [180,191–212], both of them [213–221], and uniform acceleration alone or in combinations with aforementioned fields [222–247].

A powerful probe for understanding how these extreme conditions affect strongly coupled nuclear matter is the static heavy quark-antiquark potential. Within string theory, applicable both in the holographic approach and in four-dimensional string-based effective models of QCD, this potential is computed from the world sheet action of a (classical) string, the end points of which represent the (infinitely) heavy static quark and antiquark.

Specifically, in a gauge-theory context, the expectation value of a rectangular temporal Wilson loop, $\langle W(C)\rangle$, defined over a time interval $T \to \infty$ and a spatial separation L, is governed by the dynamics of the underlying flux tube. In the limit where the flux tube is well described by a thin, classical string, the dominant contribution comes from the minimal-area world sheet spanning the contour C. This yields the relation

$$\langle W(C)\rangle \sim e^{-TV(L)} = e^{-S_{\mathrm{NG}}[\Sigma]}, \tag{1}$$

where $S_{\mathrm{NG}}[\Sigma]$ is the (renormalized) Nambu-Goto action evaluated on the corresponding surface Σ. The static quark-antiquark potential is therefore extracted as

$$V(L) = \lim_{T\to\infty} \frac{S_{\mathrm{NG}}[\Sigma]}{T}. \tag{2}$$

The key advantage of this approach is its generality: the background metric in the string action can encode not only the geometry of a holographic bulk but also the effective spacetime felt by a flux tube in a thermal, rotating, electromagnetically polarized and other medium. In this paper, we focus on arbitrary stationary spacetimes for several compelling reasons. First, a vast and physically relevant class of backgrounds is stationary: pure AdS, AdS black branes and black holes, Rindler-AdS, geometries with instantons or scalar condensates, and many solutions describing equilibrium states with rotation or external fields. Second, since we are interested in the static quark-antiquark potential ($T \to \infty$), the relevant string world sheet probes a time-independent configuration. Third, while stationary metrics retain a high degree of physical generality, their time independence substantially simplifies the equations of motion (EoM), allowing us to derive closed analytic expressions even in the presence of nondiagonal metric components. By working with a general stationary metric, we therefore obtain universal, tractable formulas for $V(L)$ that are applicable across a wide spectrum of holographic and effective string-based models of strongly coupled matter.

The paper is organized in the following way. In Sec. II, starting from arbitrary stationary spacetime, we calculate the separation distance and static potential for the quark-antiquark pair and analyze several important simplifications of the background metrics. In Sec. III, we obtain a precise analytic expression for the static quark-antiquark potential within the finite-temperature AdS/CFT framework formulated within the black brane; the details of the analytic calculation are provided in Appendix B. In Sec. IV. we review the Rindler-AdS background dual to the accelerated $\mathcal{N}=4$ super Yang-Mills plasma and find precise analytic expressions for the separation distance and static potential between quarks, the details of the analytical calculations of which we give in the Appendix C. In Sec. V, we conclude and discuss obtained results and prospects.

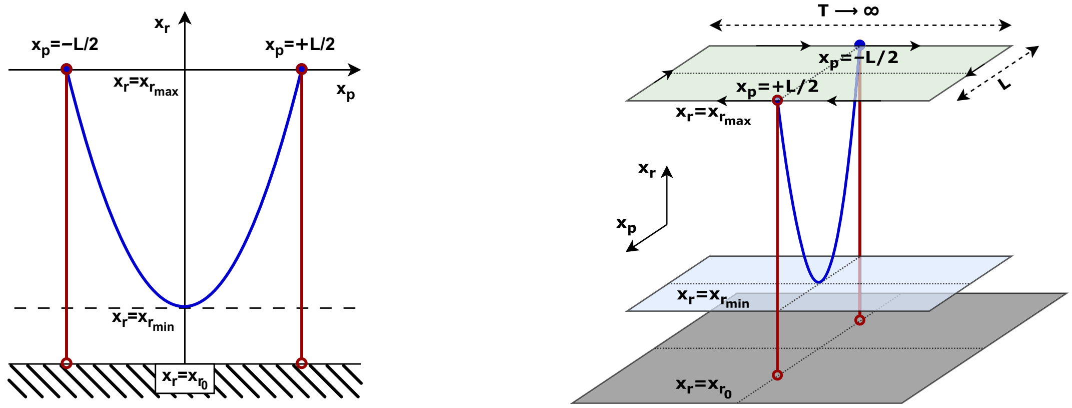

FIG. 1. The schematic representation for (1) the simple symmetric string profile and (2) the corresponding Wilson loop contour.

II. THE STATIC QUARK-ANTIQUARK POTENTIAL IN ARBITRARY STATIONARY BACKGROUND

A. The background and string configuration

We consider a D-dimensional stationary spacetime ($D \geq 3$) with the nondiagonal metric allowing for off-diagonal components that mix different spatial directions,

$$ds^2 = G_{MN} dx^M dx^N, \tag{3}$$

where the metric components G_{MN} are functions of the spatial coordinates, x_i, but independent of the time coordinate, x_0. The string propagation in such a background is governed by the Nambu-Goto action,

$$S_{\rm NG} = \frac{1}{2\pi\alpha'} \int \mathrm{d}\tau \mathrm{d}\sigma \sqrt{-g}. \tag{4}$$

Here, $1/2\pi\alpha'$ is the string tension coefficient, $\alpha' = \ell_s^2$ is the Regge slope parameter and the fundamental string length scale ℓ_s, and g is the determinant of the induced metric on the world sheet. Parametrizing the string world sheet by the coordinate pair (τ, σ), one then needs to find the induced metric tensor $g_{\alpha\beta}$, which is defined as

$$g_{\alpha\beta} = G_{MN} \partial_\alpha X^M \partial_\beta X^N, \tag{5}$$

with the embedded coordinates X^M and components of the spacetime metric G_{MN}.

We employ a static gauge choice for the string world sheet, parametrizing it in a such way that the time coordinate on the world sheet, τ, is identified with the background time, x_0. The spatial coordinate on the string world sheet, σ, is identified with a specific spatial direction in the global spacetime, x_p. The remaining coordinates, x_i with $i \neq 0, p$, are the dynamical fields $x_i(\sigma)$, describing how the string bends away from the straight line along σ. This configuration looks as follows:

$$\begin{gathered} x_0 = \tau, \qquad x_p = \sigma, \qquad x_i = x_i(\sigma), \\ x_i(\sigma = -L/2) = x_i(\sigma = +L/2) = x_{i_{\max}}, \end{gathered} \tag{6}$$

where the string end points are fixed at $\sigma = \pm L/2$ and $x_i = x_{i_{\max}}$. Hence, the distance between end points in terms of σ has a simple form,

$$L = \int_{-L/2}^{L/2} \mathrm{d}\sigma. \tag{7}$$

To avoid ambiguities in the schematic representation of the arbitrary string shape, which generally is nonsymmetric with respect to the string turning point, $x_{i_{\min}}$, and can have complex shape in several space directions, we show pictures only for a simple and clear case of the symmetric shape, where only one coordinate, x_r, depends on the string coordinate, σ, while others stay fixed, $dx_i/d\sigma = 0$ at $i \neq r$. For such cases, the string profile and the corresponding Wilson loop contour are shown in Fig. 1. We also show straight strings that run from the boundary, $x_{r_{\max}}$, up to the horizon or deep bulk limit, x_{r_0}. These strings, representing free deconfined quarks, are used later in the renormalization procedure, described in the corresponding section. The simple symmetric string profile is used for the calculations in Secs. III and IV, while in the current section we do not restrict ourself by considering such cases and will show general results for an arbitrary string configuration. For some examples of the asymmetric string configuration, see the discussion about the parity violation later in this section.

B. The equations of motion

The explicit view of the induced metric (5) in the terms of the background metric components (3) is

$$g_{\tau\tau} = G_{00}, \tag{8}$$

$$g_{\sigma\sigma} = G_{pp} + 2\sum_i G_{pi} x_i' + \sum_i \sum_j G_{ij} x_i' x_j', \tag{9}$$

$$g_{\tau\sigma} = g_{\sigma\tau} = G_{p0} + \sum_i G_{0i} x'_i, \tag{10}$$

where we denoted $x'_i = \frac{\mathrm{d}x_i}{\mathrm{d}\sigma}$. Using (8)–(10), one can write down the Lagrangian density as

$$\mathcal{L} = \sqrt{-g} = \sqrt{g_{\tau\sigma}^2 - g_{\tau\tau}g_{\sigma\sigma}} = \sqrt{-g_p - \sum_i x'_i \left[2h_{pi} + G_{00}\sum_j G_{ij}x'_j\right] + \left(\sum\nolimits_i G_{0i}x'_i\right)^2}. \tag{11}$$

Here, we introduced the following geometrical objects, which are the base terms in our work,

$$h_{ab} = G_{00}G_{ab} - G_{0a}G_{0b}, \tag{12}$$

$$g_a = h_{aa} = G_{00}G_{aa} - G_{0a}^2. \tag{13}$$

Quantity (12) characterizes a geometric coupling between directions a and b as seen by the string world sheet. For $a = b$, Eq. (13) corresponds to the determinant of the world sheet metric for a string oriented purely along the a direction. Hence, g_p in (11) defines the geometry of the background spacetime swept by the unperturbed static string oriented along the p direction. When $a \neq b$, h_{ab} describes how motions in directions a and b couple in the string dynamics, so h_{pi} in (11) reflects a geometrical connection between x_p and x_i directions. More precisely, h_{ab} is a projection metric on the spatial sections with $x_0 = \text{const}$, that is discussed later.

Using (11), we find a first integral of the EoM, which corresponds to the conserved Hamiltonian density [248],

$$\mathcal{H} = \sum\nolimits_i \mathcal{P}_i x'_i - \mathcal{L} = \frac{g_p + \sum_i h_{pi}x'_i}{\mathcal{L}} = \mathcal{C}, \tag{14}$$

where the quantities

$$\mathcal{P}_i = \frac{\partial\mathcal{L}}{\partial x'_i} = -\frac{h_{pi} + G_{00}\sum_j G_{ij}x'_j - G_{0i}\sum_j G_{0j}x'_j}{\mathcal{L}} \tag{15}$$

are the canonical momenta. For our purposes, it is sufficient to use only a set of $\mathcal{P}_i$, while other momenta are fixed via the Virasoro constraints, see Appendix A. The constant $\mathcal{C}$ is defined from the boundary condition at the string turning point, where all the coordinate derivatives vanish: $x'_i|_{x_i = x_{i_{\min}}} = 0$. Substituting this condition into (14) and solving for $\mathcal{C}$ yields

$$\mathcal{C} = -\sqrt{-g_p}|_{x_i = x_{i_{\min}}} = -\sqrt{G_{0p}^2 - G_{00}G_{pp}}|_{x_i = x_{i_{\min}}}. \tag{16}$$

One finds that the canonical momenta in Eq. (15), evaluated at the string turning point, are constant,

$$\mathcal{P}_i|_{x_i = x_{i_{\min}}} = -\frac{h_{pi}}{\sqrt{-g_p}}\bigg|_{x_i = x_{i_{\min}}} = \frac{1}{\mathcal{C}}h_{pi}\bigg|_{x_i = x_{i_{\min}}}. \tag{17}$$

These vanish for spacetimes with certain symmetries satisfying $h_{pi} = 0$ (the simplest case is the diagonal metric).

Now it is convenient to split coordinates x_i into radial, x_r, and transverse, x_i $(i \neq r)$, directions to change the integration variable σ to x_r via $\mathrm{d}\sigma = \mathrm{d}x_r/x'_r$. To solve for the derivative x'_r, we begin by squaring both sides of Eq. (14) to eliminate the square root present in the Lagrangian $\mathcal{L}$,

$$\frac{(g_p^{(T)})^2 + 2g_p^{(T)}h_{pr}x'_r + h_{pr}^2 x_r'^2}{\mathcal{L}_T^2 - g_r x_r'^2 - 2x'_r[h_{pr} - G_{0r}\sum_{i\neq r}G_{0i}x'_i]} = \mathcal{C}^2,$$

where we defined

$$g_r = h_{rr} = G_{00}G_{rr} - G_{0r}^2, \tag{18}$$

$$g_p^{(T)} = g_p + \sum\nolimits_{i\neq r} h_{pi}x'_i, \tag{19}$$

$$\mathcal{L}_T^2 = \mathcal{L}^2|_{x'_r = 0} = -g_p - \sum_{i\neq r} x'_i \left[2h_{pi} + G_{00}\sum_{j\neq r} G_{ij}x'_j\right] + \left(\sum\nolimits_{i\neq r} G_{0i}x'_i\right)^2. \tag{20}$$

Here, $\mathcal{L}_T$ is the Lagrangian density for a purely transverse string profile with $x'_r = 0$, $g_p^{(T)}$ a modification of (13) that takes into account the transverse corrections of the string shape and g_r the determinant of the induced metric for a string oriented purely along the radial direction.

Then, by collecting terms with the same powers of x'_r, we obtain a quadratic equation,

$$a x_r'^2 + b x'_r + c = 0, \tag{21}$$

with the following coefficients:

$$a = h_{pr}^2 + \mathcal{C}^2 g_r,$$
$$b = 2\left[g_p^{(T)} h_{pr} + \mathcal{C}^2\left(h_{pr} - G_{0r}\sum\nolimits_{i\neq r} G_{0i} x_i'\right)\right],$$
$$c = (g_p^{(T)})^2 - \mathcal{C}^2 \mathcal{L}_T^2.$$

The solution of Eq. (21) is given by a standard expression,

$$x_r' = \frac{-b \pm \sqrt{b^2 - 4ac}}{2a}. \tag{22}$$

For instance, in the background family with $h_{pr} = 0$ for string configurations with a simple transverse shape $x_i' = 0$ (see Fig. 1). the general expression for x_r' simplifies to

$$x_r'^2 = -\frac{g_p(g_p + \mathcal{C}^2)}{\mathcal{C}^2 g_r}, \tag{23}$$

while considering the diagonal metrics leads to

$$x_r'^2 = -\frac{G_{pp}(G_{00}G_{pp} + \mathcal{C}^2)}{\mathcal{C}^2 G_{rr}}. \tag{24}$$

C. Possible source of the parity violation

For an arbitrary stationary background $h_{pr} \neq 0$, a consideration of the simple string ansatz with $x_i' = 0$ leads to the following view of EoM (22):

$$x_r' = \frac{\sqrt{g_p + \mathcal{C}^2}}{h_{pr}^2 + \mathcal{C}^2 g_r}\left(-h_{pr}\sqrt{g_p + \mathcal{C}^2} \pm |\mathcal{C}|\sqrt{-h}\right), \tag{25}$$

where we defined $h = -(h_{pr}^2 - g_r g_p) = -(h_{pr}^2 - h_{rr}h_{pp})$, the meaning of which we find below. Note that Eq. (25) is generally nonsymmetric with respect to the string turning point. Hence, a nonzero value of the quantity h_{pr} signals a breakdown of symmetry of the string profile along the involved directions, which may be related to the parity violation.

As we noted earlier, h_{pr} reflects space asymmetry in the p–r plane. The physical meaning of h becomes especially clear when the stationary metric is written in the standard form with splitting along the timelike Killing field,

$$\mathrm{d}s^2 = G_{00}(\mathrm{d}t + A_a \mathrm{d}x^a)^2 + \frac{h_{ab}}{G_{00}}\mathrm{d}x^a \mathrm{d}x^b, \tag{26}$$

where G_{00} is the norm of the timelike Killing field, and $A_a = G_{0a}/G_{00}$ is the gravitomagnetic potential, so h_{pr} defines the geometry of the spatial sections. Hence,

$$h = -(h_{pr}^2 - h_{rr}h_{pp}) = \det\begin{pmatrix} h_{pp} & h_{pr} \\ h_{pr} & h_{rr} \end{pmatrix}$$
$$= G_{00}\det\begin{pmatrix} G_{00} & G_{0p} & G_{0r} \\ G_{0p} & G_{pp} & G_{pr} \\ G_{0r} & G_{pr} & G_{rr} \end{pmatrix} \tag{27}$$

is the determinant of the projection metric on spatial sections with $x_0 = \tau = \mathrm{const}$. In the parametrization (26), h_{pr} combines two possible sources of parity violation: nonzero off-diagonal metric element $G_{pr} \neq 0$ and a presence of the gravitomagnetic fields $A_p \neq 0$, $A_r \neq 0$. For instance, it may correspond to pseudoscalar condensates or some stationary flows.

Consequently, the asymmetry of the string profile, the source of which is $h_{pr} \neq 0$, may probe a parity violation in the quark-antiquark interaction. A quantitative measure of this violation can be provided by a shift of the string turning point away from the midpoint between the quark and antiquark, which is computed from the first integral of the equations of motion.

As an example of a background with $h_{pr} \neq 0$, one can consider the Kerr-AdS$_5$ solution (in the static-at-infinity frame [249]):

$$\mathrm{d}s^2 \sim -(1 + y^2\ell^{-2})\mathrm{d}T^2 + \frac{\mathrm{d}y^2}{1 + y^2\ell^{-2} - \frac{2M}{\Delta^2 y^2}}$$
$$+ \frac{2M}{\Delta^3 y^2}(\mathrm{d}T - a\sin^2\Theta\mathrm{d}\Phi - b\cos^2\Theta\mathrm{d}\Psi)^2$$
$$+ y^2(\mathrm{d}\Theta^2 + \sin^2\Theta\mathrm{d}\Phi^2 + \cos^2\Theta\mathrm{d}\Psi^2), \tag{28}$$

with angles $0 \leq \Theta \leq \frac{\pi}{2}$, $0 \leq \Phi, \Psi \leq 2\pi$, and

$$\Delta = 1 - a^2\ell^{-2}\sin^2\Theta - b^2\ell^{-2}\cos^2\Theta. \tag{29}$$

Here, a and b are two independent rotation parameters in orthogonal planes, which can give rise to a pseudoscalar (axial) structure in spacetime through the topological invariants of the curved geometry, such as $R\tilde{R}$, which change sign under parity reflection. Indeed, parametrizing the string profile by $(x_p, x_r) = (\Phi, \Psi)$ or $(x_p, x_r) = (\Psi, \Phi)$, one obtains $h_{pr} \neq 0$:

$$h_{pr} = -\frac{abM\sin^2 2\Theta}{2\Delta^3 y^2}\left(1 + \frac{y^2}{\ell^2}\right). \tag{30}$$

As follows from the equation of motion (25), this non-zero h_{pr} generates two distinct branches for the string profile, which explicitly manifest parity breaking in the static gauge.

When $h_{pr} = 0$, the profile becomes symmetric; however, this condition does not necessarily restore full parity

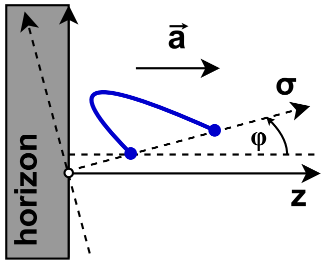

FIG. 2. The asymmetric string configuration in the 4D Rindler space.

invariance of the background: it may merely reflect a specific compensation or a configuration that is insensitive to the existing symmetry violations. Moreover, one should be mindful that h_{pr} is not a diffeomorphism-invariant scalar: its non-zero value in the chosen parametrization signals parity violation, but the invariant physical content of the latter should be extracted from appropriate curvature invariants or conserved quantities.

For instance, one can consider the usual 4D Rindler space,

$$\mathrm{d}s^2 = -a^2 z^2 \mathrm{d}t^2 + \mathrm{d}x^2 + \mathrm{d}y^2 + \mathrm{d}z^2. \tag{31}$$

This background belongs to the family with $h_{pr} = 0$ for any pair (x_p, x_r). We show an asymmetric string configuration in Fig. 2, where the world sheet coordinate σ is chosen such that the string is oriented at some angle ϕ to the acceleration axis z. Here, the asymmetry is evident; however, even in an apparently "straight" configuration with $\sigma = z$—where the string is stretched purely along the acceleration axis without sagging—the energy density remains nonhomogeneous. Although the spatial shape in (x, y, z) coordinates is a straight line, the energy per unit coordinate length (or the effective local tension) decreases toward the horizon. From the perspective of an observer constantly accelerating in the Rindler wedge, the parity is manifestly broken by the restriction to a noninertial frame and the limited accessible region.

D. General expression for the static potential

Expressing $\mathcal{L}$ via $\mathcal{C}$ from (14), one can simplify the action (4),

$$S_{\mathrm{NG}} = \frac{\mathcal{T}}{2\pi\alpha' \mathcal{C}} \int_{-L/2}^{L/2} \mathrm{d}\sigma \left(g_p^{(T)} + h_{pr} x_r'\right). \tag{32}$$

Taking into account that the EoM (25) generally is not symmetric with respect to the string turning point $x_{r_{\min}}$, we rewrite expressions (7) and (32) as

$$L = \int_{x_{r_{\min}}}^{x_{r_{\max}}} \mathrm{d}x_r \left(\frac{1}{x'_{r_+}} + \frac{1}{x'_{r_-}}\right), \tag{33}$$

$$S_{\mathrm{NG}} = \frac{\mathcal{T}}{2\pi\alpha' \mathcal{C}} \left[\int_{x_{r_{\min}}}^{x_{r_{\max}}} \mathrm{d}x_r \left(\frac{g_p^{(T)}}{x'_{r_+}} + \frac{g_p^{(T)}}{x'_{r_-}} + 2h_{pr}\right)\right], \tag{34}$$

where we denoted two different branches by $x_{r_\pm}$.

The Nambu-Goto action (34) typically exhibits divergence that requires renormalization. For asymptotically AdS spaces (and other geometries with similar ultraviolet behavior), this is accomplished by subtracting the action of two straight, disconnected strings extending from the boundary to the deep infrared (see red straight lines in Fig. 1),

$$S_0 = \frac{\mathcal{T}}{\pi\alpha'} \int_{x_{r_0}}^{x_{r_{\max}}} \mathrm{d}x_r \sqrt{-g_r} = \frac{\mathcal{T}}{\pi\alpha'} \left(\int_{x_{r_0}}^{x_{r_{\min}}} + \int_{x_{r_{\min}}}^{x_{r_{\max}}}\right) \mathrm{d}x_r \sqrt{-g_r}, \tag{35}$$

with g_r defined in Eq. (18), and x_{r_0} denoted the infrared end point: either a horizon radius or, in horizon-free geometries, the deep bulk limit. Hence, the following expression for the renormalized action can be obtained:

$$S_{\mathrm{NG}}^{\mathrm{ren}} = S_{\mathrm{NG}} - S_0 = \frac{\mathcal{T}}{\pi\alpha'} \left[\frac{1}{2\mathcal{C}} \int_{x_{r_{\min}}}^{x_{r_{\max}}} \mathrm{d}x_r \left(\frac{g_p^{(T)}}{x'_{r_+}} + \frac{g_p^{(T)}}{x'_{r_-}} + 2h_{pr} - 2\mathcal{C}\sqrt{-g_r}\right) - \int_{x_{r_0}}^{x_{r_{\min}}} \mathrm{d}x_r \sqrt{-g_r}\right]. \tag{36}$$

Finally, associating the string with a heavy quark-antiquark pair, the static potential energy (2) can be explicitly written as

$$\pi\alpha' V = \frac{1}{2\mathcal{C}} \int_{x_{r_{\min}}}^{x_{r_{\max}}} \mathrm{d}x_r \left(\frac{g_p^{(T)}}{x'_{r_+}} + \frac{g_p^{(T)}}{x'_{r_-}} + 2h_{pr} - 2\mathcal{C}\sqrt{-g_r}\right) - \int_{x_{r_0}}^{x_{r_{\min}}} \mathrm{d}x_r \sqrt{-g_r}, \tag{37}$$

which is a general expression obtained within string theory for a general static string configuration in an arbitrary stationary

D-dimensional background. The obtained result does not depend on whether one works within the framework of the holographic models or the effective description of the static QCD fields between a heavy quark pair.

Note that without additional assumptions, confident simplifications of (37) are not justified. For example, while one may postulate string symmetry about the string turning point $x_{r_{\min}}$, such a symmetric profile may not represent the minimum-energy configuration when the metric coupling h_{pr} is nonzero [see Eq. (25) and discussions later]. Although symmetric solutions might exist in special cases even for $h_{pr} \neq 0$, rigorous confidence in this symmetry requires $h_{pr} = 0$.

E. Isolation of the linear-in-distance term for some background families

It is easy to see that the general formulas (33) and (37) are reduced to particular cases obtained in the literature earlier. For instance, for diagonal metrics with an account of (24), it simplifies to

$$L = 2|\mathcal{C}| \int_{x_{r_{\min}}}^{x_{r_{\max}}} dx_r \sqrt{-G_{00}G_{rr}} \frac{1}{\sqrt{G_{00}G_{pp}(G_{00}G_{pp} + \mathcal{C}^2)}}, \tag{38}$$

$$\pi\alpha' V = \int_{x_{r_{\min}}}^{x_{r_{\max}}} \mathrm{d}x_r \sqrt{-G_{00}G_{rr}} \left(\frac{\sqrt{G_{00}G_{pp}}}{\sqrt{G_{00}G_{pp} + \mathcal{C}^2}} - 1 \right) - \int_{x_{r_0}}^{x_{r_{\min}}} \mathrm{d}x_r \sqrt{-G_{00}G_{rr}} \tag{39}$$

$$= -\frac{\mathcal{C}L}{2} + \int_{x_{r_{\min}}}^{x_{r_{\max}}} \mathrm{d}x_r \sqrt{-G_{00}G_{rr}} \left(\sqrt{1 + \frac{\mathcal{C}^2}{G_{00}G_{pp}}} - 1 \right) - \int_{x_{r_0}}^{x_{r_{\min}}} \mathrm{d}x_r \sqrt{-G_{00}G_{rr}}, \tag{40}$$

where we used the following identity:

$$\frac{x}{\sqrt{x^2+1}} = \frac{\sqrt{x^2+1}}{x} - \frac{1}{x\sqrt{x^2+1}}. \tag{41}$$

Equation (40) is exactly the same as obtained in [137], taking into account a relation between the constant definitions ($\mathcal{C} = -c$).

For the Schwarzschild-AdS$_5$ and Kerr-AdS$_5$ black holes considered in [204], we also receive the same expressions (see Eqs. (3.12) and (3.32) in [204]). In fact, these black hole solutions are the members of the background family with $h_{pr} = 0$, and for the string configurations with fixed transverse shape, $x_i' = 0$, shown in Fig. 1, we can isolate the linear part in the potential using (23) and (41),

$$L = 2|\mathcal{C}| \int_{x_{r_{\min}}}^{x_{r_{\max}}} \mathrm{d}x_r \sqrt{-g_r} \frac{1}{\sqrt{g_p(g_p + \mathcal{C}^2)}}, \tag{42}$$

$$\pi\alpha' V = \int_{x_{r_{\min}}}^{x_{r_{\max}}} \mathrm{d}x_r \sqrt{-g_r} \left(\frac{\sqrt{g_p}}{\sqrt{g_p + \mathcal{C}^2}} - 1 \right) - \int_{x_{r_0}}^{x_{r_{\min}}} \mathrm{d}x_r \sqrt{-g_r} \tag{43}$$

$$= -\frac{\mathcal{C}L}{2} + \int_{x_{r_{\min}}}^{x_{r_{\max}}} \mathrm{d}x_r \sqrt{-g_r} \left(\sqrt{1 + \frac{\mathcal{C}^2}{g_p}} - 1 \right) - \int_{x_{r_0}}^{x_{r_{\min}}} \mathrm{d}x_r \sqrt{-g_r}. \tag{44}$$

The result (44) also means that for such backgrounds (with $h_{pr} = 0$) the Nambu-Goto action for a simple static symmetric string configuration ($x_i' = 0$, $x_r' \neq 0$) can be initially written as

$$S_{\mathrm{NG}} = \frac{\mathcal{T}}{\pi\alpha'} \left(-\frac{\mathcal{C}L}{2} + \int_{x_{r_{\min}}}^{x_{r_{\max}}} \mathrm{d}x_r \sqrt{-g_r} \sqrt{1 + \frac{\mathcal{C}^2}{g_p}} \right), \tag{45}$$

with $\mathcal{C}$ and L defined in (16) and (42), correspondingly.

III. THE QUARK-ANTIQUARK POTENTIAL VIA ADS/CFT AT FINITE TEMPERATURE

A. The potential and separation distance in the black brane background

A straightforward generalization of the first calculations [128,129] of the static potential energy of the quark-antiquark pair, performed in the conformal background of the pure AdS space in the large-N limit, to the finite temperature case was carried out in [130]. The background for such a case consists of the N coincident D3-branes (the black brane) and looks as

$$\mathrm{d}s^2 = -f(U)\frac{U^2}{\mathcal{R}^2}\mathrm{d}t^2 + \frac{1}{f(U)}\frac{\mathcal{R}^2}{U^2}\mathrm{d}U^2 + \frac{U^2}{\mathcal{R}^2}\mathrm{d}x_p^2 + \mathcal{R}^2\mathrm{d}\Omega_{d-2}, \tag{46}$$

with the blackening function $f(U) = 1 - U_T^4/U^4$ and AdS curvature $\mathcal{R} = \sqrt{4\pi gN}$. The parameter $U_T^4 = \frac{27}{3}\pi^4 g^2 \mu$, expressed via the energy density above extremality on the brane μ, and the coupling constant g, is related to the Hawking temperature as $T_{\mathrm{H}} = U_T/(\pi\mathcal{R}^2)$.

In this section, following our general formulas from Sec. II, we obtain precise analytic expressions for the separation, L, and static potential, V, for the quark-antiquark pair in the large-N limit and then analyze their different temperature limits. We use the following string configuration:

$$\tau = t, \qquad \sigma = x_p, \qquad x_r = U = U(\sigma), \\ U(\sigma \pm L/2) = U_{\max} = \infty, \tag{47}$$

the schematic representation of which is shown in Fig. 1. The basic units for the calculations are

$$g_p = G_{tt}G_{xx} = -f(U)\frac{U^4}{R^4} = \frac{1}{R^4}(U_T^4 - U^4), \tag{48}$$

$$g_r = G_{tt}G_{rr} = -1, \tag{49}$$

$$\mathcal{C} = -\sqrt{-g_p}|_{U=U_m} = -\frac{1}{R^2}\sqrt{U_m^4 - U_T^4}, \tag{50}$$

where U_m is the coordinate of the string turning point. Using these units and Eqs. (42)–(44), one can find the following expressions for L and V (see details of the calculations in Appendix B):

$$L = \frac{\mathcal{R}^2}{U_m}\frac{\pi}{\sqrt{2}\beta}\sqrt{1-z}\,{}_2F_1\left(\frac{1}{2},\frac{3}{4};\frac{5}{4};z\right), \tag{51}$$

$$\pi\alpha' V = U_T + U_m(1-z)\frac{\pi}{\sqrt{2}\beta}\left[\frac{1}{2}{}_2F_1\left(\frac{1}{2},\frac{3}{4};\frac{5}{4};z\right) - {}_2F_1\left(\frac{3}{4},\frac{3}{2};\frac{5}{4};z\right)\right] \tag{52}$$

$$= U_T - \frac{U_m^2}{\mathcal{R}^2}\sqrt{1-z}\left(\frac{1+z}{1-z}\frac{L}{2} + 2z\frac{\partial L}{\partial z}\right). \tag{53}$$

Here, ${}_2F_1(a,b;c;x)$ is the Gauss hypergeometric function, and we introduced a convenient shorthand notation,

$$z = U_T^4/U_m^4, \tag{54}$$

and coefficient,

$$\beta = \frac{\Gamma(\frac{1}{4})^2}{4\sqrt{\pi}} = \frac{\pi}{2}{}_2F_1\left(\frac{1}{2},\frac{1}{2};1;\frac{1}{2}\right) = K\left(\frac{1}{2}\right), \tag{55}$$

which is actually the elliptic integral of the first kind,

$$K(m) = \int_0^1 \mathrm{d}x \frac{1}{\sqrt{(1-x^2)(1-mx^2)}}, \tag{56}$$

with elliptic modulus $k = \sqrt{m} = 1/\sqrt{2}$. The formulas (51) and (52) were also obtained in Ref. [250]; however, the authors did not recognize the expression (53).

It is exciting that the potential (53) is expressed completely in terms of the quarks separation, L, and its derivative, $\frac{\partial L}{\partial z}$. The derivative with respect to z carries a direct physical meaning when one recalls that the temperature at a given bulk depth U_m is redshifted. The local temperature at some point U is given by the Tolman-Ehrenfest law,

$$T(U) = \frac{T_{\mathrm{H}}}{\sqrt{-G_{tt}(U)}} = \frac{1}{\pi\mathcal{R}}\frac{U_T}{U}\frac{1}{\sqrt{f(U)}}. \tag{57}$$

In turn, the local temperature at the string turning point, U_m, is

$$T(U_m) = \frac{1}{\pi\mathcal{R}}\frac{z^{1/4}}{\sqrt{1-z}}. \tag{58}$$

Consequently, the derivative $\frac{\partial L}{\partial z}$ quantifies how the quark-antiquark separation changes as the local temperature at the string turning point varies. Finally, rewriting $U_T = \pi\mathcal{R}^2 T_{\mathrm{H}}$ and $U_m = \frac{\mathcal{R}}{\sqrt{2}}\frac{T_{\mathrm{H}}}{T_m}\sqrt{1+\sqrt{1+4\pi^4\mathcal{R}^4T_m^4}}$, it is possible to express Eqs. (51)–(53) in terms of the Hawking, T_{H}, and local, $T_m = T(U_m)$, temperatures as

$$L = \frac{1}{\sqrt{2}\pi\beta}\frac{\sqrt{z}}{\mathcal{R}T_mT_{\mathrm{H}}}{}_2F_1\left(\frac{1}{2},\frac{3}{4};\frac{5}{4};z\right), \tag{59}$$

$$\pi\alpha' V = \pi\mathcal{R}^2T_{\mathrm{H}} + \frac{\pi}{\sqrt{2}\beta}\frac{\mathcal{R}T_{\mathrm{H}}}{T_m}\sqrt{1-z}\left[\frac{1}{2}{}_2F_1\left(\frac{1}{2},\frac{3}{4};\frac{5}{4};z\right) - {}_2F_1\left(\frac{3}{4},\frac{3}{2};\frac{5}{4};z\right)\right] \tag{60}$$

$$= \pi\mathcal{R}^2T_{\mathrm{H}} - \frac{T_{\mathrm{H}}^2}{T_m^2}\frac{1}{\sqrt{1-z}}\left(\frac{1+z}{1-z}\frac{L}{2} + 2z\frac{\partial L}{\partial z}\right). \tag{61}$$

B. The screening length and critical separation distance

We show dependencies of the potential and distance between quarks in Fig. 3 for several values of the Hawking temperature T_{H}. To avoid dimensions, we express all the quantities in terms of the curvature $\mathcal{R}$, so it is easy to restore all dimensions setting the dimension for $\mathcal{R}$. Also the potential is multiplied by $\pi\alpha'$ to keep arbitrariness of α'.

As one can see, opposite to the conformal case at zero temperature, where the potential and distance have only one branch, the presence of the finite temperature leads to the double-valued behavior for such quantities. From the physical point of view, the maximum attainable separation between the quark and antiquark is the screening length, beyond which the interaction is practically turned off. The value of the string turning point at the screening length, U_s, is simply related to the parameter U_T as

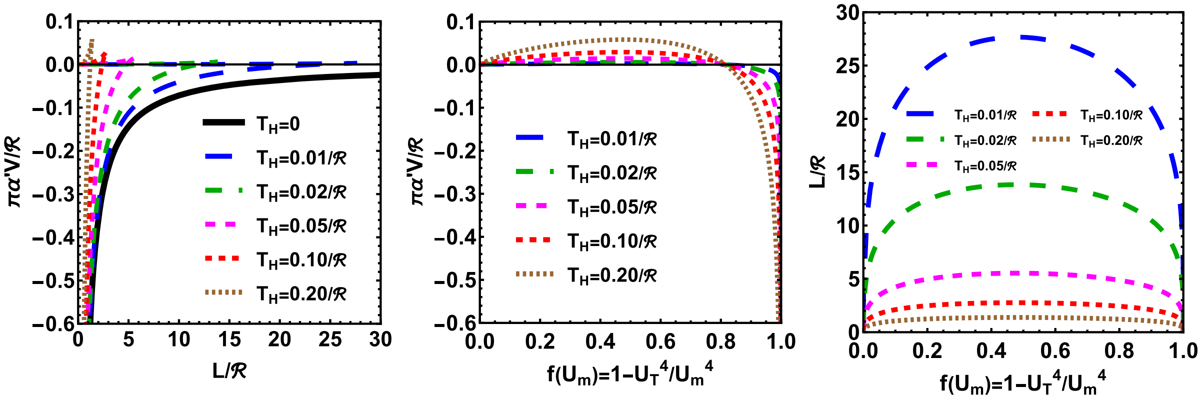

FIG. 3. Numerical calculations for (1) the quark-antiquark potential V (52) depending on the distance L (51) between quark, (2) the potential V as a function of $f(U_m)$, and (3) the distance L as a function of $f(U_m)$. Different line colors and styles, corresponding to different values of the Hawking temperature, are shown in the legends. All the quantities are expressed in terms of the AdS curvature $\mathcal{R}$ to avoid the dimensions. For plot (1), we also show the zero-temperature results by a black solid curve.

$$U_s = 2^{1/4} U_T, \tag{62}$$

at which point the blackening function takes a middle value, $f(U_s) = 1/2$, and the local temperature depends only on the curvature $\mathcal{R}$,

$$T_s = T(U_s) = \frac{2^{1/4}}{\pi \mathcal{R}}. \tag{63}$$

The lower branch of the potential corresponds to the case of $U_m > U_s$ and at $V < 0$ reflects the bound state for the quark-antiquark pair—quarkonium. Starting from a some point U_c, where the static potential vanishes, $V(U_c) = 0$, there is a metastable bound state of the system for a parameters in range of $U_c \geq U_m > U_s$. For such cases, the U-shaped string configuration, corresponding to a confined pair of quarks, is energetically disfavored compared with a pair of disconnected straight strings that run from the boundary down to the horizon, the latter representing two independent, deconfined quarks, on which the quarkonium can dissociate via tunneling or thermal fluctuations. The value of U_c may be well estimated as

$$U_c^{\mathrm{approx}} = \left(\frac{4\sqrt{2}\sqrt{\pi}}{\beta}\right)^{1/4} U_T,$$

$$T_c = T(U_c) \approx \frac{1}{\pi \mathcal{R}} \frac{\left(\frac{4\sqrt{2}\sqrt{\pi}}{\beta}\right)^{1/4}}{\sqrt{1 - \frac{4\sqrt{2}\sqrt{\pi}}{\beta}}}. \tag{64}$$

However, it is not a precise value of the solution for $V(U_c) = 0$ and the ratio of our estimation, U_c^{approx}, to a precise solution, U_c, is $U_c^{\mathrm{approx}}/U_c \approx 0.9991$, but practically, the difference is insignificant. Moreover, the quark separation at this point, $L(U_c)$, is slightly smaller than the screening length, see Fig. 4. The upper branch with $U_m < U_s$ corresponds to completely unstable configuration in which the string turning point lies too close to the horizon, U_T. In this regime, any small fluctuation causes the middle area of the string to be irreversibly pulled into the horizon, effectively dissociating the quarkonium.

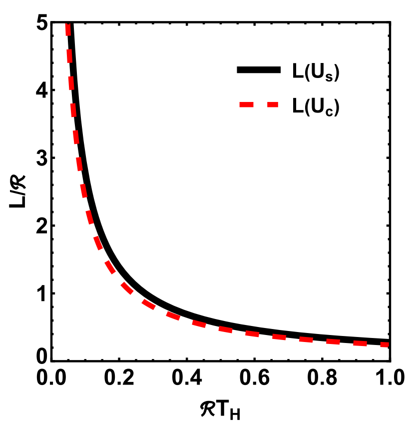

FIG. 4. The screening length, $L(U_s)$, depicted by solid black line, and the critical distance, $L(U_c)$, depicted by red dashed line, as functions of the Hawking temperature, T_{H}. All the quantities are expressed in terms of the AdS curvature $\mathcal{R}$ to avoid the dimensions.

C. The small temperature limit

In the zero-temperature limit ($T_{\mathrm{H}} = U_T = z = 0$), our calculation yields an exact agreement with the results of Refs. [128–130],

$$L_0 = \frac{\pi}{\sqrt{2}\beta} \frac{\mathcal{R}^2}{U_m} = \frac{2\sqrt{2}\pi^{3/2}}{\Gamma(\frac{1}{4})^2} \frac{\mathcal{R}^2}{U_m}, \tag{65}$$

$$V_0 = -\frac{\pi}{4\beta^2} \frac{\mathcal{R}^2}{L_0} = -\frac{4\pi^2}{\Gamma(\frac{1}{4})^4} \frac{\mathcal{R}^2}{L_0} = -\frac{1}{2\sqrt{2}\beta} U_m = -\frac{\sqrt{2\pi}}{\Gamma(\frac{1}{4})^2} U_m, \tag{66}$$

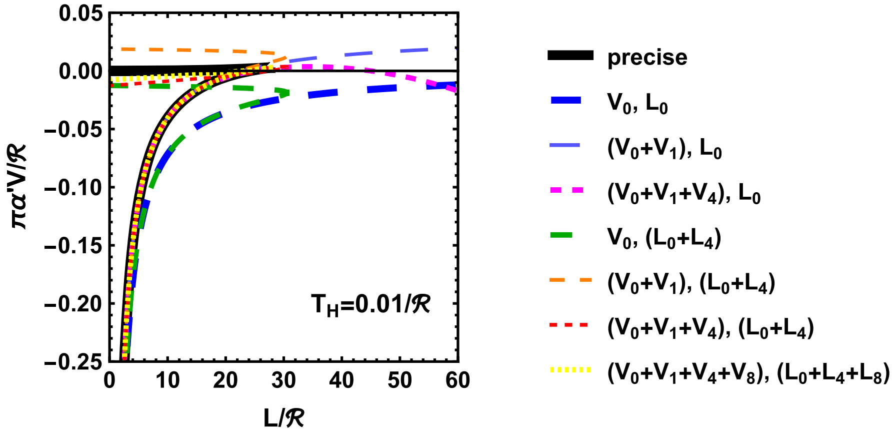

FIG. 5. The dependence of the potential from the series expansion (67) as a function of the separation L from the expansion (68) at the fixed Hawking temperature $T_{\mathrm{H}} = 0.01/\mathcal{R}$. Different terms of the expansions, indexed in terms of the temperature powers, are depicted in the legend. All the quantities are expressed in terms of the AdS curvature $\mathcal{R}$ to avoid the dimensions.

where we set $\alpha' = 1$ for clarity. The series expansion at the small temperatures looks as

$$L_{T_{\mathrm{H}}\approx 0} = L_0 - \frac{4\beta^4}{5}(L_0 T_{\mathrm{H}})^4 - \frac{8\beta^8}{5}(L_0 T_{\mathrm{H}})^8 - \frac{160\beta^{12}}{39}(L_0 T_{\mathrm{H}})^{12} + O(T_{\mathrm{H}}^{16}), \tag{67}$$

$$V_{T_{\mathrm{H}}\approx 0} = V_0 - \frac{4\beta^2}{\pi}(L_0 T_{\mathrm{H}}) + 2\beta^4(L_0 T_{\mathrm{H}})^4 + \frac{6\beta^8}{5}(L_0 T_{\mathrm{H}})^8 + \frac{28\beta^{12}}{15}(L_0 T_{\mathrm{H}})^{12} + O(T_{\mathrm{H}}^{16}), \tag{68}$$

where the coefficient β is given by (55). The conformal nature of the theory reveals itself in the fact that VL can depend on T_{H} only through the combination LT_{H}, as noted in Ref. [130]. However, the actual combination is $L_0 T_{\mathrm{H}}$, due the fact that L itself depends on the temperature. Also, in [130], the lowest correction term $\sim L_0 T_{\mathrm{H}}$ was missed (see Eq. (8) in [130]), but it comes from $U_T = \pi\mathcal{R}^2 T_{\mathrm{H}}$ after the renormalization procedure.

To analyze the series expansions (67) and (68), we plot different terms with respect to the temperature powers in Fig. 5. At small separations, the string world sheet remains close to the conformal boundary, $U_m \gg U_T$, where the blackening function is $f(U_m) \approx 1$. In this region, the metric (46) is close to the pure AdS, and the system exhibits approximate conformal invariance. Consequently, the leading behavior of the potential is universal and coincides with the zero-temperature Coulomb form, $V \approx V_0 \sim \frac{1}{L_0}$. As the separation increases, the string probes deeper into the bulk, eventually reaching the region where $f(U_m)$ deviates significantly from unity. The full nonlinear dependence on temperature, encoded in the metric, then becomes essential, and the precise forms of the potential and distance are sensitive to higher-order terms in the temperature expansions. Note that the "swallowtail" behavior of the potential and separation distance is caused by temperature corrections for the separation only. The universal small-L behavior is thus a robust UV feature, while the near-critical region reflects the detailed IR deformation of the conformal theory by the thermal scale.

IV. THE QUARK-ANTIQUARK POTENTIAL IN THE RINDLER-ADS SPACE

A. The Rindler-AdS background

In this section, we clarify the influence of acceleration on the quarkonium dissociation within the holographic approach. One need to consider the Rindler-AdS space, the dual of which is the $\mathcal{N} = 4$ supersymmetric Yang-Mills (SYM) theory. The Rindler-AdS spacetime has been widely investigated in [222,230,233,236,246]. The heavy quark-antiquark potential in the presence of acceleration was previously calculated for the $\mathcal{N} = 2$ confining SYM theory in [227], and for $\mathcal{N} = 4$ SYM in [228]; however, here we present a more comprehensive study, including the first precise analytic expressions.

The Rindler-AdS metric is given by the following expression:

$$\mathrm{d}s^2 = -a_c^2\xi^2\mathrm{d}t^2 + \frac{\mathrm{d}\xi^2}{1 + a_c^2\xi^2} + (1 + a_c^2\xi^2) \times \left[\mathrm{d}\chi^2 + \frac{1}{a_c^2}\sinh^2(a_c\chi)\mathrm{d}\Omega_{d-2}^2\right]. \tag{69}$$

For a qualitative analysis, one often sets the coordinate Rindler acceleration equal to the inverse AdS radius, $a_c = 1/\mathcal{R}$ (see, for instance, Ref. [236]). The numerical value of a_c itself is not a physical invariant (it can be changed by rescaling the coordinates), but the AdS radius $\mathcal{R}$ provides the intrinsic geometric scale of the spacetime. The quantity

$a_c = 1/\mathcal{R}$ then carries a correct dimension of the acceleration and serves as a natural reference value.

In the limit $a_c\xi \longrightarrow 0$, the metric (69) reduces to the line element of flat Rindler space with a horizon at $\xi = 0$,

$$\mathrm{d}s^2 = -a_c^2\xi^2\mathrm{d}t^2 + \mathrm{d}\xi^2 + \mathrm{d}\chi^2 + \chi^2\mathrm{d}\Omega_{d-2}^2. \quad (70)$$

The coordinates (69) describe a region satisfying $(X^1)^2 - (X^0)^2 > 0$ and $(X^1)^2 - (X^{d+1})^2 > 0$ in a $(d+2)$-dimensional embedding Minkowski space with two timelike directions,

$$-(X^0)^2 + (X^1)^2 + \cdots + (X^d)^2 - (X^{d+1})^2 = -\mathcal{R}^2, \quad (71)$$

which possesses the symmetry group $O(2,d)$, corresponding to AdS_{d+1}. This embedding shows that the Rindler observers in AdS follow hyperbolic trajectories in the ambient Minkowski space; i.e., they are also Rindler observers with respect to the embedding space.

At $\xi \longrightarrow \infty$, the metric (69) asymptotically approaches the conformal boundary of AdS,

$$\mathrm{d}s_{\mathrm{boundary}}^2 = -\mathrm{d}t^2 + \mathrm{d}\chi^2 + \frac{1}{a_c^2}\sinh^2(a_c\chi)\mathrm{d}\Omega_{d-2}^2, \quad (72)$$

which is the metric on $\mathbb{R}\times\mathbb{H}^{d-1}$, where the hyperbolic spatial section $\mathbb{H}^{d-1}$ has a curvature radius of $1/a_c = \mathcal{R}$. Moreover, for any finite ξ, the induced metric on a constant-ξ hypersurface is also conformally equivalent to $\mathbb{R}\times\mathbb{H}^{d-1}$. This reflects the fact that the Rindler-AdS foliation preserves the conformal structure of the boundary at every finite ξ, even though the holographic dual CFT in the AdS/CFT sense is usually defined only on the ideal conformal boundary attached at $\xi \longrightarrow \infty$.

As it known from the general relativity, the temperature seen by an observer moving with constant acceleration is not always proportional to the proper acceleration. For the Rindler-AdS space, the proper acceleration of an observer at constant ξ is given by

$$a_{\mathrm{prop}}^2 = a_{\mathrm{loc}}^2 + a_c^2 = \frac{1}{\xi^2} + \frac{1}{\mathcal{R}^2}, \quad (73)$$

where the local acceleration is defined as $a_{\mathrm{loc}} = \frac{1}{\xi}$. In work [222], a general formula for the local temperature in $(\mathrm{A})\mathrm{dS}_{d+1}$ was obtained,

$$T_{\mathrm{loc}} = \frac{1}{2\pi}\sqrt{\frac{2\Lambda}{d(d-1)} + a_{\mathrm{prop}}^2} = \frac{a_{\mathrm{embed}}}{2\pi}, \quad (74)$$

where a_{embed} is the proper acceleration of the Rindler observer in the flat embedding space, and Λ is the cosmological constant.

For AdS_{d+1}, the cosmological constant looks as $\Lambda = -\frac{1}{\mathcal{R}^2}\frac{d(d-1)}{2}$; therefore, the condition for a real value of the temperature requires the proper acceleration to satisfy $a_{\mathrm{prop}} \geq \frac{1}{\mathcal{R}} = a_{\mathrm{crit}}$, where we defined a critical acceleration a_{crit}. The observers with $a_{\mathrm{prop}} > a_{\mathrm{crit}}$ possess a nondegenerate Rindler-type horizon and measure a nonzero local temperature (74), which can be rewritten as

$$T(\xi) = T_{\mathrm{loc}} = \frac{1}{2\pi}\sqrt{a_{\mathrm{prop}}^2 - a_{\mathrm{crit}}^2}. \quad (75)$$

At $a_{\mathrm{prop}} = a_{\mathrm{crit}}$, the horizon becomes extremal (zero surface gravity), and the local temperature vanishes. As an example, such an observer is located at $\xi \longrightarrow \infty$. Finally, observers with $a_{\mathrm{prop}} < a_{\mathrm{crit}}$ have no causal horizon. Their trajectories are globally extendible, and they do not perceive a thermal spectrum.

Remarkably, the critical acceleration coincides exactly with the parameter that appears in the Rindler-AdS metric (69), i.e., $a_{\mathrm{crit}} = a_c$. The proper acceleration (73) is always greater than or equal to a_c. Thus, the Rindler-AdS coordinate system naturally covers only the worldlines of supercritical (and asymptotically critical) observers. The parameter a_c in the metric therefore has a clear physical interpretation: it sets both the AdS curvature scale $\mathcal{R}$ and the minimal acceleration required for an observer to possess a horizon and a well-defined temperature in AdS.

Using (73), one can obtain a final expression for the local temperature,

$$T(\xi) = T_{\mathrm{loc}} = \frac{1}{2\pi\xi}. \quad (76)$$

Remarkably, this is precisely the same expression as for an accelerated detector in flat Rindler space, despite the nonzero curvature of AdS. The horizon at $\xi = 0$ possesses the Hawking temperature T_{H}, defined via its surface gravity. For the Rindler-AdS metric, one finds $T_{\mathrm{H}} = a_c/(2\pi) = 1/(2\pi\mathcal{R})$, so the local temperature (76) can then be written as

$$T(\xi) = \frac{T_{\mathrm{H}}}{\sqrt{-G_{tt}(\xi)}} = \frac{1}{2\pi\xi}, \quad (77)$$

which is exactly the Tolman-Ehrenfest law for temperature distribution in a static gravitational field. Thus, while the horizon itself has a fixed temperature T_{H}, an accelerated observer at finite ξ experiences a higher local temperature due to gravitational redshift.

B. Influence of the acceleration on the static quark-antiquark potential

Choosing the following string ansatz,

$$\tau = t, \qquad \sigma = \chi, \qquad \xi = \xi(\sigma), \\ \xi(\sigma = \pm L/2) = \xi_{\max} = \infty, \tag{78}$$

corresponding to a simple symmetric string shape depicted in Fig. 1, one can find our main quantities for the potential and distance expressions,

$$g_p = G_{tt}G_{\chi\chi} = -a_c^2\xi^2(1 + a_c^2\xi^2), \tag{79}$$

$$g_r = G_{tt}G_{\xi\xi} = -\frac{a_c^2\xi^2}{1 + a_c^2\xi^2}. \tag{80}$$

The first integral takes the following value:

$$\mathcal{C} = -a_c\xi_m\sqrt{1 + a_c^2\xi_m^2}, \tag{81}$$

where the physical value of the string turning point, ξ_m, satisfying $\xi \geq 0$, $\mathcal{C}^2 \geq 0$, $a_c > 0$, is given by

$$\xi_m = \frac{\sqrt{\sqrt{4\mathcal{C}^2 + 1} - 1}}{\sqrt{2}a_c}. \tag{82}$$

In the special case of an acceleration $a_c = 1/\xi_m$, the first integral is a universal constant $\mathcal{C} = -\sqrt{2}$.

Now, using (79)–(82), one can analytically calculate the integrals in the expressions for the distance (42) and potential (44) between quarks. Direct calculations (see Appendix C for details) lead to the following expressions for the distance L and potential V:

$$L = 2\xi_m\mathrm{Re}\left[\tilde{\Pi}(n, m) - \frac{K(1-m)}{1-n}\right], \tag{83}$$

$$\pi\alpha' V = \frac{1}{a_c} + \sqrt{\frac{1}{a_c^2} + \xi_m^2}\,\mathrm{Re}[iK(m) - \tilde{E}(m)] \tag{84}$$

$$= \frac{1}{a_c} - \frac{\mathcal{C}L}{2} + \frac{\xi_m\mathcal{C}}{n}\mathrm{Re}[\tilde{K}(m) - n\tilde{\Pi}(n, m) - \tilde{E}(m)], \tag{85}$$

where we introduced linear combinations of the complete elliptic integrals

$$\tilde{\Pi}(n, m) = m\Pi(1-n, 1-m) + i\Pi(n, m), \tag{86}$$

$$\tilde{K}(m) = mK(1-m) + iK(m), \tag{87}$$

$$\tilde{E}(m) = E(1-m) + iE(m), \tag{88}$$

with the characteristic n, elliptic modulus k, and parameter m given by

$$n = -a_c^2\xi_m^2, \qquad m = k^2 = \frac{n}{1-n}. \tag{89}$$

It was tested that the expressions (83)–(85) give the same result as direct numerical integrations of (83) and (44) in the Rindler-AdS case. Notably, the elliptic integrals in the context of the static interquark potential are also arisen in different setups, for instance, [251,252].

Calculations of the asymptotic behavior lead to the following expressions:

$$T_{\mathrm{H}} \sim a_c = \frac{1}{\mathcal{R}} \longrightarrow 0: \qquad L \sim \hat{L} = 2\xi_m\log\left(\frac{4}{a_c\xi_m}\right), \\ V \sim \frac{a_c\xi_m}{4}(\hat{L} - 3\xi_m) = \frac{\sqrt{\pi}}{2\sqrt{2}}\sqrt{\frac{|V_0|}{L_0}}(\hat{L} + 6\sqrt{2}\beta V_0); \tag{90}$$

$$T_{\mathrm{H}} \sim a_c = \frac{1}{\mathcal{R}} \longrightarrow \infty: \qquad L \sim L_0, \qquad V \sim V_0 \sim -\frac{1}{L_0}, \tag{91}$$

where L_0 and V_0 are the conformal results in pure AdS defined in (65) and (66), correspondingly, and β is given by (55). Interestingly, the high-temperature (large acceleration or small curvature) limit in the Rindler-AdS asymptotically comes to the results for a conformal case of pure AdS. The opposite limit is related to the logarithmic divergencies caused by a singularity in the metric (69).

To compare different AdS geometries (different radii $\mathcal{R}$) while keeping a fixed reference length ℓ, it is convenient to introduce a dimensionless scaling parameter a_0 via the relation $a_c = a_0/\ell$, where ℓ is a fixed reference length, for example, the AdS radius of a chosen "reference" geometry (so that $a_0 = 1$ in that case). This parametrization emphasizes that, when ℓ is held fixed, the dimensionless number a_0 distinguishes one geometry from another, whereas a_c (or equivalently $1/\mathcal{R}$) absorbs the dimensional dependence.

Consequently, physical observables should depend on acceleration only through dimensionless combinations. For example, in the final part of this section, we see that the quark-antiquark potential, written as dimensionless function, a_cV, of the dimensionless distance between quarks, a_cL, is independent of the specific numerical choice of a_0, which is a direct consequence of the unphysical nature of a_c. On the other hand, the dimensionless ratio V/ℓ expressed as a function of L/ℓ retains an explicit dependence on a_0, thereby reflecting how the underlying geometry changes with the rescaled acceleration parameter.

We show dependencies of the potential and distance between quarks in the Rindler-AdS background in Fig. 6 for several values of the acceleration parameter $a_0 = a_c\ell = 0.4,\ 0.6,\ 1,\ 2$. To avoid dimensions, we express all the quantities in terms of ℓ. Also, the potential is multiplied by $\pi\alpha'$ to keep arbitrariness of α'.

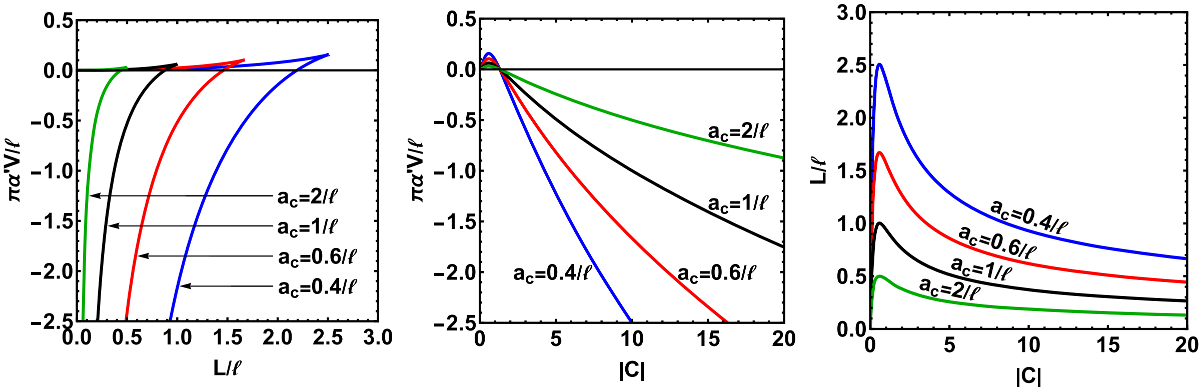

FIG. 6. Numerical calculations in the Rindler-AdS background (69) for (1) the quark-antiquark potential V (44) depending on the distance L (42) between quarks. (2) the potential V as a function of the absolute value of constant $\mathcal{C}$, and (3) the distance L as a function of the absolute value of constant $\mathcal{C}$. Different line colors correspond to different values of the acceleration: blue for $a_c = 0.4/\ell$, red for $a = 0.6/\ell$, black for $a_c = 1/\ell$, and green for $a_c = 2/\ell$.

Again, one can observe a double-valued behavior for the potential and separation distance, so we refer to Sec. III for the explanation. However, now a critical value of the string turning point, ξ_c, at which the potential takes a zero value, $V(\xi_c)$, is related to the acceleration/curvature as

$$\xi_c = \frac{3}{\pi a_c} = \frac{3\mathcal{R}}{\pi}, \tag{92}$$

where the temperature is

$$T_c = \frac{\pi}{3} T_{\mathrm{H}} = \frac{a_c}{6}, \tag{93}$$

that is depicted by a red dashed line in the contour plots in Fig. 7. Note that it is slightly higher (the factor is ≈ 1.05) than the horizon temperature T_{H}, which is depicted by a black/white line in Fig. 7.

The parameter relation for the separation length can be find from the condition $\frac{\partial V(a_c,\xi_m)}{\partial \xi_m}|_{\xi_m=\xi_s} = 0$, from which one finds

$$E\left(\frac{1+a_c^2\xi_s^2}{1+2a_c^2\xi_s^2}\right) = \frac{1}{2} K\left(\frac{1+a_c^2\xi_s^2}{1+2a_c^2\xi_s^2}\right). \tag{94}$$

The approximate solution of (94) and corresponding temperature are

$$\xi_s \approx \frac{0.5163}{a_c}, \qquad T_s = T(\xi_s) \approx \frac{a_c}{2\pi \cdot 0.5163}, \tag{95}$$

which are shown in Fig. 7 by a green dashed line.

In Fig. 8, we also show three-dimensional plots of the distance and potential in the acceleration–temperature at the string turning point plane. As one can see, at low acceleration a_0 and temperatures $T(\xi_m)$, the distance and

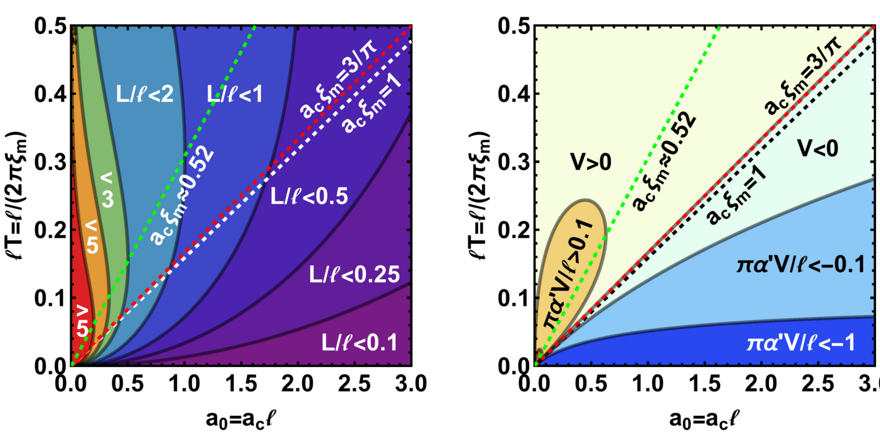

FIG. 7. Contour plots of the distance L (first pane) and potential V (second pane) between quarks as functions of the dimensionless acceleration parameter $a_0 = a_c\ell$ and of the dimensionless temperature at the string turning point $\ell T = \ell/(2\pi\xi_m)$. Different values of V or L, corresponding certain contours, are depicted by colors and labels. Different dashed lines correspond to several important relations between a_c and ξ_m: green for the screening length (95), red for $V = 0$, and black/white for the Hawking temperature T_{H}.

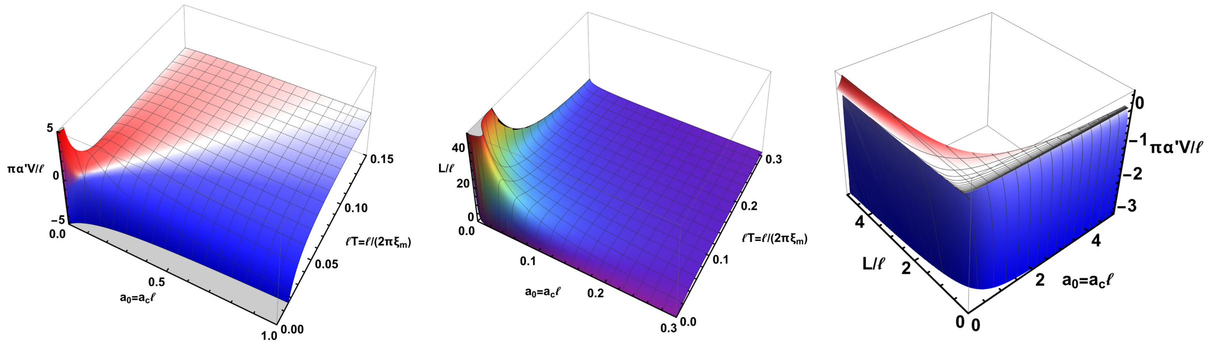

FIG. 8. Three-dimensional plots of the distance L (first panel) and potential V (second panel) between quarks as functions of the dimensionless acceleration parameter $a_0 = a_c\ell$ and of the dimensionless temperature at the string turning point $\ell T = \ell/(2\pi\xi_m)$; the potential V as a function of the distance L and acceleration parameter a_0 (third panel).

potential undergo faster growth and diverge in the limit of $a_c \longrightarrow 0$ and $T(\xi_m) \longrightarrow 0$.

An accelerated observer in a Rindler wedge has access only to the part of spacetime limited by its horizon. As acceleration increases, the observer moves closer to the horizon. Two accelerated quarks, in order to remain in causal connection with each other, must be closer to each other; otherwise, the horizon will break the string between them. The critical distance at which the string can exist decreases with increasing acceleration, see Fig. 6. The shorter string is in a more "compressed" state. The energy stored in the string per unit length (tension) is constant, but due to the curvature of spacetime and the horizon influence, the effective energy that must be expended to separate the quarks increases. This manifests itself as an increase in the interquark potential, which can be seen in Fig. 6.

Hence, the characteristic temperature increases with the acceleration $a_c = a_0/\ell = 1/\mathcal{R}$. This occurs either by increasing the dimensionless parameter a_0 at fixed curvature scale ℓ, or by decreasing ℓ at fixed a_0, which is the same as the AdS horizon $\mathcal{R}$ decrease. However, one can argue that the acceleration parameter a_c is unphysical, so a certain value of this sets only the scale between time and space coordinates. One can perform a transformation of the coordinates in the Rindler-AdS metric (69) and redefine the originally chosen acceleration value a_c to another value or even get rid of the acceleration by the coordinate transformation $\tilde{x}_i = a_c x_i$.

Indeed, the potential scaled onto acceleration value, $\tilde{V} = a_c V$, as a function of the acceleration-scaled distance, $\tilde{L} = a_c L$, shows no dependence on the certain acceleration value a_c, see Fig. 9. Similar scaling is also observed in the lattice QCD calculations [253,254]. In such terms, the Hawking temperature is a universal constant $\tilde{T}_H = 1/2\pi$, which does not depend on the acceleration or AdS radius values. Hence, the characteristic temperatures are also constants: $\tilde{T}_c = (\pi/3)\tilde{T}_H = 1/6$ and $\tilde{T}_s \approx 1/(2\pi \cdot 0.5163)$.

For a comparison, we also show results obtained in Sec. III at several values of the Hawking temperatures. As one can see, scaled results in the Rindler-AdS space are

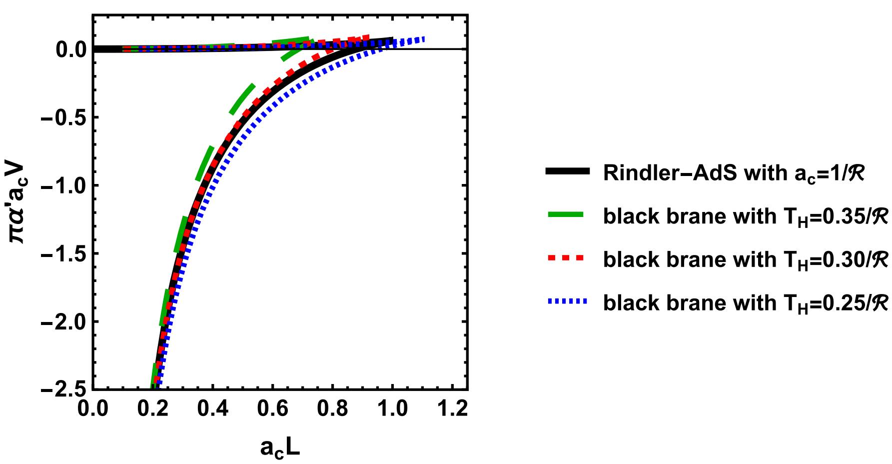

FIG. 9. The scaled onto acceleration potential, $\tilde{V} = a_c V$, as a function of the acceleration-scaled distance, $\tilde{L} = a_c L$. Results in the black brane background (51)–(52) are also shown at different Hawking temperatures, $\mathcal{R}T_{\mathrm{H}} = T_{\mathrm{H}}/a_c = 0.35, 0.30, 0.25$, depicted in the legend.

very close to the results in the black brane background at $\mathcal{R}T_{\mathrm{H}} = T_{\mathrm{H}}/a_c \approx 0.3$.

V. CONCLUSIONS

In this paper, we have presented calculations of the separation distance and static potential energy for a heavy quark-antiquark pair within string theory for an arbitrary stationary background. We established that for a simple U-shaped string with only radial dependence on the space string coordinate, $x_r'(\sigma) \neq 0$, the string is generally not symmetric with respect to the turning point, and the symmetry (at least for the EoM) restores only for backgrounds with a single constraint: $h_{pr} = G_{00}G_{pr} - G_{0p}G_{0r} = 0$. Consequently, such asymmetric strings may probe a possibility of the parity violation in the quark-antiquark interaction, taking into account that confident evidences of the violation should be extracted from other appropriate invariant quantities.

Nevertheless, we obtained general expressions for the distance (33) and potential (37) within a nonsymmetric arbitrary string profile. Then, we show that for a simple string ansatz (only radial dependency $x_i' = 0$, $x_r' \neq 0$ and symmetry with respect to the turning point, see Fig. 1) one can directly isolate a linear-in-distance term even for complicated nondiagonal metrics with the only one constraint ($h_{pr} = 0$), see Eq. (44). It is a wide class of the backgrounds, including simple diagonal (or semidiagonal with respect to p and r as for the AdS family solutions) cases, stationary metrics, special cases with $G_{pr} = \frac{G_{0p}G_{0r}}{G_{00}}$, where one can diagonalize this metric part by a simple time shift depending on r and p, etc. It also means that one can initially work with a simplified version of the Nambu-Goto action, expressed in terms of the first integral and the distance between string end points (quarks), see (45).

As a first example, we apply our general formulas to the AdS/CFT at a finite temperature formulated in terms of N coincident D3-branes (the black brane), which are in the large-N limit dual to the finite-temperature $\mathcal{N} = 4$ SYM plasma. We obtained precise analytic expressions for the separation distance (51) and static potential (52) in terms of the hypergeometric functions. We noted that the potential may be expressed in terms of the separation and its derivative by temperature, see Eqs. (53) or (61) for an expression obtained completely in temperature terms. We found values of the parameters and temperatures at the critical separation and screening length and analyze their dependence on the Hawking temperature. Performing a small-temperature expansion, it was shown that the series coefficients are expressed in terms of the dimensionless product of the separation distance in the conformal limit and Hawking temperature, L_0T_{H}, and the "swallowtail" behavior of the potential and distance are caused by temperature corrections for the separation distance.

In the last part of the work, within the framework of the holographic duality between the Rindler-AdS space and the accelerated $\mathcal{N} = 4$ SYM plasma, we find analytic expressions for the distance (83) and static potential (84) and (85) between quarks in terms of the elliptic integrals. Analyzing their asymptotics, we observed that the high Hawking temperature (high acceleration or small curvature) limits of the Rindler-AdS results come to the conformal expressions obtained for a pure AdS. We show that the distance between quarks decreases, the static potential between them increases, and the characteristic temperatures, $T_c = (\pi/3)T_H = a_c/6$ and $T_s \approx a_c/(2\pi \cdot 0.5163)$, increase with an acceleration, a_c. However, we observe that an acceleration-scaled potential, $\tilde{V} = a_cV$, as a function of the acceleration-scaled distance, $\tilde{L} = a_cL$, does not depend on the certain value of the acceleration, a_c. This result, reflecting self-similarity of the holographic setup, can be also obtained in the dimensionless metric after rescaling of the coordinates onto the acceleration, $\tilde{x}_i = a_cx_i$, for which one obtains universal values of the characteristic temperatures.

Finally, we want to note that the interquark potential obtained in the Rindler-AdS background has a similar dependence on the distance as in the case of the pure AdS [128], D-brane [130], and D instanton [205] in the AdS space, the Schwarzschild-AdS and Kerr-AdS black holes [204], and other cases [136,190,206,250,251]. Therefore, we can conclude that this is a common feature of the simple string ansatz (78) in the AdS-like backgrounds.

ACKNOWLEDGMENTS

We are grateful to V. Braguta, E. Kolomeitsev, and A. Golubtsova for the valuable discussions. The work was supported by the grant of the Foundation for the Advancement of Theoretical Physics and Mathematics "BASIS" No. 25-1-5-80-1.

DATA AVAILABILITY

There are no publicly available research data or software supporting this paper. Requests for further information or data should be sent to the authors.

APPENDIX A: THE VIRASORO CONSTRAINTS

The Nambu-Goto action has invariance under reparametrization ($\tau, \sigma \longrightarrow \tilde{\tau}, \tilde{\sigma}$), but it will be lost after fixing of the gauge. To restore this symmetry and eliminate unphysical degrees of freedom, one must impose the Virasoro constraints, which require the vanishing of the world sheet stress-energy tensor.

Let us start from the general Lagrangian density without any constraints on the background and string configuration,

$$\tilde{\mathcal{L}} = \sqrt{-(\dot{X}^\mu \dot{X}_\mu)(X'^\nu X'_\nu) + (\dot{X}^\mu X'_\mu)^2}, \qquad \text{(A1)}$$

where we denoted $\dot{x} = \partial x/\partial\tau$ and $x' = \partial x/\partial\sigma$. In the Polyakov approach, the Virasoro constraints can be found by nullifying of the Hilbert stress-energy tensor, but for the Nambu-Goto action the tensor is trivial because the induced metric $g_{ab} = G_{MN}\partial_a X^M \partial_b X^N$ is not an independent variable. In such a case, we must use the Noether's theorem, where one finds the Canonical stress-energy tensor,

$$\Theta^a_b = \frac{\partial\tilde{\mathcal{L}}}{\partial(\partial_a X^\mu)}\partial_b X^\mu - \delta^a_b\tilde{\mathcal{L}}. \tag{A2}$$

The explicit view of the components is

$$\begin{aligned}\Theta^\tau_\tau &= \frac{\partial\tilde{\mathcal{L}}}{\partial\dot{X}^\mu}\dot{X}^\mu - \tilde{\mathcal{L}} = \mathcal{P}^{(\tau)}_\mu\dot{X}^\mu - \tilde{\mathcal{L}},\\ \Theta^\tau_\sigma &= \frac{\partial\tilde{\mathcal{L}}}{\partial\dot{X}^\mu}X'^\mu = \mathcal{P}^{(\tau)}_\mu X'^\mu,\end{aligned} \tag{A3}$$

$$\begin{aligned}\Theta^\sigma_\sigma &= \frac{\partial\tilde{\mathcal{L}}}{\partial X'^\mu}X'^\mu - \tilde{\mathcal{L}} = \mathcal{P}^{(\sigma)}_\mu X'^\mu - \tilde{\mathcal{L}},\\ \Theta^\sigma_\tau &= \frac{\partial\tilde{\mathcal{L}}}{\partial X'^\mu}\dot{X}^\mu = \mathcal{P}^{(\sigma)}_\mu\dot{X}^\mu.\end{aligned} \tag{A4}$$

Now, we come back to the stationary background (3), fix the gauge, and nullify the components of Θ^a_b,

$$\begin{aligned}\Theta^\tau_\tau &= \mathcal{P}^{(\tau)}_\mu\dot{X}^\mu - \tilde{\mathcal{L}} = \mathcal{P}^{(\tau)}_0 - \mathcal{L} = 0,\\ \Theta^\tau_\sigma &= \mathcal{P}^{(\tau)}_\mu X'^\mu = \mathcal{P}^{(\tau)}_i x'^i = 0,\end{aligned} \tag{A5}$$

$$\begin{aligned}\Theta^\sigma_\sigma &= \mathcal{P}^{(\sigma)}_i X'^\mu - \tilde{\mathcal{L}} = \mathcal{P}_p + \mathcal{P}_i x'^i - \mathcal{L} = 0,\\ \Theta^\sigma_\tau &= \mathcal{P}^{(\sigma)}_\mu\dot{X}^\mu = \mathcal{P}_0 = 0.\end{aligned} \tag{A6}$$

Here, $\mathcal{P}^{(\sigma)}_\mu \longrightarrow \mathcal{P}_\mu$, $\tilde{\mathcal{L}} \longrightarrow \mathcal{L}$, $X_i \longrightarrow x_i$ are our common notations in the paper.

Finally, we obtain the Virasoro constraints for our general string configuration in arbitrary stationary background,

$$\mathcal{P}^{(\tau)}_0 = \mathcal{L}, \qquad \mathcal{P}^{(\tau)}_i x'^i = 0, \tag{A7}$$

$$\mathcal{P}_p = -\mathcal{P}_i x'^i + \mathcal{L} = -\mathcal{H} = -\mathcal{C}, \qquad \mathcal{P}_0 = 0, \tag{A8}$$

where we used the expression for the (reduced) Hamiltonian density with the constant $\mathcal{C}$ fixed by the string turning point in the configuration, see (6), (14), and (16). As one can see, total Hamiltonian density is zero (A5), but the reduced one (A7) is constant, which is more convenient quantity for calculations. Hence, in any case of the string configuration like (6) in a stationary background, one can simply use our general expressions obtained in Sec. II without any problems with the Virasoro constraints.

APPENDIX B: ANALYTIC CALCULATIONS IN THE ADS/CFT AT FINITE TEMPERATURE

Inserting (48) into (42) leads to

$$\begin{aligned}L &= 2|\mathcal{C}|\int_{U_m}^{\infty} dU\sqrt{\frac{-g_r}{g_p(g_p+C^2)}}\\ &= 2\mathcal{R}^2\sqrt{U_m^4 - U_T^4}\int_{U_m}^{\infty} dU\frac{1}{\sqrt{(U_T^4 - U^4)(U_m^4 - U^4)}}\\ &= //x = \frac{U_T}{U}; \qquad dU = -U_T\frac{dx}{x^2}; \qquad x_0 = \frac{U_T}{U_m}//\\ &= 2\frac{\mathcal{R}^2}{U_T^3}\sqrt{U_m^4 - U_T^4}\frac{x^3}{3}F_1\left(\frac{3}{4};\frac{1}{2},\frac{1}{2};\frac{7}{4};x^4,\frac{x^4}{x_0^4}\right)\Big|_0^{x_0}\\ &= \frac{\mathcal{R}^2}{U_m}\frac{\pi}{\sqrt{2}\beta}\sqrt{1-z}\,{}_2F_1\left(\frac{1}{2},\frac{3}{4};\frac{5}{4};z\right),\end{aligned} \tag{B1}$$

where $F_1(a;b_1,b_1;c;x,y)$ is the Appell hypergeometric function of two variables, ${}_2F_1(a,b;c;x)$ is the Gauss hypergeometric function, and we show a temporary variable transformation inside the double slashes. Here, we also introduced a convenient shorthand notation,

$$z = U_T^4/U_m^4, \tag{B2}$$

and coefficient,

$$\beta = \frac{\Gamma(\frac{1}{4})^2}{4\sqrt{\pi}} = \frac{\pi}{2}{}_2F_1\left(\frac{1}{2},\frac{1}{2};1;\frac{1}{2}\right) = K\left(\frac{1}{2}\right), \tag{B3}$$

which is actually the elliptic integral of the first kind,

$$K(m) = \int_0^1 \mathrm{d}x\frac{1}{\sqrt{(1-x^2)(1-mx^2)}}, \tag{B4}$$

with the elliptic modulus $k = \sqrt{m} = 1/\sqrt{2}$.

The expression for the potential may be calculated in a similar way. After a paste of (48) into (43), one obtains

$$\begin{aligned}\pi\alpha' V &= \int_{U_m}^{\infty} dU\sqrt{-g_r}\left(\sqrt{\frac{g_p}{g_p+C^2}} - 1\right) - \int_{U_m}^{U_T} dU\sqrt{-g_r}\\ &= \int_{U_m}^{\infty} dU\left(\sqrt{\frac{U_T^4 - U^4}{U_m^4 - U^4}} - 1\right) - U_m + U_T\\ &= //x = \frac{U_T}{U}; \qquad dU = -U_T\frac{dx}{x^2}; \qquad x_0 = \frac{U_T}{U_m}//\\ &= U_T\int_0^{x_0}\frac{dx}{x^2}\left(\sqrt{\frac{1-x^4}{1-\frac{x^4}{x_0^4}}} - 1\right) - U_m + U_T\end{aligned}$$

$$= U_T - U_m + U_T \left[\frac{3x^7}{7x_0^4} F_1 \left(\frac{7}{4}; \frac{1}{2}, \frac{1}{2}; \frac{11}{4}; x^4, \frac{x^4}{x_0^4} \right) - \frac{x^3}{3} \left(1 + \frac{2}{x_0^4} \right) F_1 \left(\frac{3}{4}; \frac{1}{2}, \frac{1}{2}; \frac{7}{4}; x^4, \frac{x^4}{x_0^4} \right) + \frac{1}{x} \left(1 + \sqrt{1-x^4} \sqrt{1 - \frac{x^4}{x_0^4}} \right) \right] \Bigg|_0^{x_0}$$

$$= U_T + U_m (1-z) \frac{\pi}{\sqrt{2}\beta} \left[\frac{1}{2} {}_2F_1 \left(\frac{1}{2}, \frac{3}{4}; \frac{5}{4}; z \right) - {}_2F_1 \left(\frac{3}{4}, \frac{3}{2}; \frac{5}{4}; z \right) \right]. \tag{B5}$$

One can recognize a linear-in-distance term in the potential due to the first hypergeometric function. Moreover, it is possible to express the second hypergeometric function in terms of the first one, hence, express the potential in terms of the distance explicitly. Using the following identity:

$$ {}_2F_1 \left(\frac{3}{4}, \frac{3}{2}; \frac{5}{4}; z \right) = {}_2F_1 \left(\frac{1}{2}, \frac{3}{4}; \frac{5}{4}; z \right) + 2z \frac{d}{dz} {}_2F_1 \left(\frac{1}{2}, \frac{3}{4}; \frac{5}{4}; z \right), \tag{B6}$$

we obtain the final view of the potential,

$$\pi \alpha' V = U_T - \frac{U_m^2}{\mathcal{R}^2} \sqrt{1-z} \left[\frac{L}{2} + \frac{2\sqrt{1-z}}{U_m} z \frac{d}{dz} \left(\frac{U_m L}{\sqrt{1-z}} \right) \right],$$
$$= U_T - \frac{U_m^2}{\mathcal{R}^2} \sqrt{1-z} \left(\frac{1+z}{1-z} \frac{L}{2} + 2z \frac{\partial L}{\partial z} \right). \tag{B7}$$

It is easy to check that an application of the second formula (44) leads to the same result as above.

APPENDIX C: ANALYTIC CALCULATIONS IN THE RINDLER-ADS BACKGROUND

First, inserting (79)–(82) into (42) leads to the following expression for the distance between string end points L:

$$\begin{aligned} L &= 2|\mathcal{C}| \int_{\xi_m}^{\infty} \frac{\mathrm{d}\xi}{1 + a_c^2 \xi^2} \frac{1}{\sqrt{a_c^2 \xi^2 (1 + a_c^2 \xi^2) - \mathcal{C}^2}} \\ &= //x = a_c \xi; x_m = a_c \xi_m // = \frac{2|\mathcal{C}|}{a_c} \int_{a_c \xi_m}^{\infty} \frac{\mathrm{d}x}{1 + x^2} \frac{1}{\sqrt{(x^2 - x_m^2)(x^2 + x_m^2 + 1)}} \\ &= //y = \frac{x}{x_m}; \qquad n = -x_m^2; \qquad m = k^2 = \frac{n}{1-n} // = 2i\xi_m \int_1^{\infty} \frac{\mathrm{d}y}{1 - ny^2} \frac{1}{\sqrt{(1-y^2)(1-my^2)}} \\ &= 2i\xi_m \Pi(\arcsin y; n, m)|_{y=1}^{y \longrightarrow \infty}, \end{aligned} \tag{C1}$$

where for clarity we show auxiliary variable redefinitions inside the double slashes. Here, we also introduced

$$\Pi(z; n, m) = \int_0^z \mathrm{d}x \frac{1}{(1 - nx^2)\sqrt{(1-x^2)(1-mx^2)}}, \tag{C2}$$

$$\Pi(n, m) = \Pi(z = \pi/2; n, m), \tag{C3}$$

which are the incomplete and complete elliptic integrals of the third kind, correspondingly, with the characteristic n and elliptic modulus $k = \sqrt{m}$.

One can note that $n = -a_c^2 \xi_m^2 < 0$ and $m = k^2 = n/(1-n) < 0$, so the modulus k is complex valued. While this representation is mathematically well defined, the analytic continuation of elliptic integrals to complex parameters introduces branch ambiguities, so to avoid this problem, we take the real part of the analytically continued expression. Using the identity for the asymptotic behavior of the elliptic integral of the third kind with imaginary argument,

$$\begin{aligned}\lim_{\alpha\longrightarrow\infty}\Pi(-i\alpha;n,m) &= i\,\frac{F(-\pi/2;1-m)-n\Pi(-\pi/2;1-n,1-m)}{1-n}\\ &= -i\,\frac{n\Pi(1-n,1-m)-K(1-m)}{1-n},\end{aligned} \tag{C4}$$

we can evaluate the upper limit explicitly. Substituting this into our expression for the proper length yields

$$\begin{aligned}L &= 2\xi_m\mathrm{Re}\left[\frac{n\Pi(1-n,1-m)-K(1-m)}{1-n}+i\Pi(n,m)\right]\\ &= 2\xi_m\mathrm{Re}\left[\tilde{\Pi}(n,m)-\frac{K(1-m)}{1-n}\right],\end{aligned} \tag{C5}$$

where we introduced the following shorthand notation:

$$\tilde{\Pi}(n,m) = m\Pi(1-n,1-m)+i\Pi(n,m). \tag{C6}$$

Similarly, one can calculate an analytic formula for the potential. After direct substitution of (79)–(82) into (43), we obtain

$$\pi\alpha' V = \int_{\xi_m}^{\infty}\mathrm{d}\xi\,\frac{a_c^2\xi^2}{\sqrt{\mathcal{C}^2-a_c^2\xi^2(1+a_c^2\xi^2)}}-\int_0^{\infty}\mathrm{d}\xi\,\frac{a_c\xi}{\sqrt{1+a_c^2\xi^2}},$$

where the calculations of the second integral are straightforward,

$$\int_0^{\infty}\mathrm{d}\xi\,\frac{a_c\xi}{\sqrt{1+a_c^2\xi^2}} = \sqrt{\frac{1}{a_c^2}+\xi^2}\,\Bigg|_{\xi=0}^{\xi\longrightarrow\infty}. \tag{C7}$$

The first integral is calculated in a similar way as (C1), namely,

$$\begin{aligned}\int_{\xi_m}^{\infty}\mathrm{d}\xi\,\frac{a_c^2\xi^2}{\sqrt{\mathcal{C}^2-a_c^2\xi^2(1+a_c^2\xi^2)}} &= //y=\xi/\xi_m,\qquad n=-a_c^2\xi_m^2,\qquad m=k^2=\frac{n}{1-n}//\\ &= i\sqrt{\frac{1}{a_c^2}+\xi_m^2}\left[\int_1^{\infty}\mathrm{d}y\,\frac{\sqrt{1-my^2}}{\sqrt{1-y^2}}-\int_1^{\infty}\mathrm{d}y\,\frac{1}{\sqrt{(1-y^2)(1-my^2)}}\right]\\ &= i\sqrt{\frac{1}{a_c^2}+\xi_m^2}\,[E(\arcsin y;m)-F(\arcsin y;m)]\Bigg|_{y=1}^{y\longrightarrow\infty},\end{aligned}$$

where

$$F(z;m) = \int_0^z \mathrm{d}x\,\frac{1}{\sqrt{(1-x^2)(1-mx^2)}}, \tag{C8}$$

$$E(z;m) = \int_0^z \mathrm{d}x\,\frac{\sqrt{1-mx^2}}{\sqrt{1-x^2}}, \tag{C9}$$

are the incomplete elliptic integrals of the first and second kind, correspondingly. In turn, at the lower bound $y=1$, one comes to the complete integrals of the first, $K(m)$, and second, $E(m)$, kinds,

$$K(m) = F(z=\pi/2;m), \tag{C10}$$

$$E(m) = E(z = \pi/2; m). \tag{C11}$$

At the upper integration bound $y \longrightarrow \infty$, one can use the following limit for $F(z; m)$:

$$\lim_{y\longrightarrow\infty} F(\arcsin y; m) = -iK(1 - m), \tag{C12}$$

while for $E(z; m)$ one must explicitly perform the imaginary-argument transformation,

$$E(i\phi; m) = i\bigg(F(\psi; 1 - m) - E(\psi; 1 - m) + \tan\psi\sqrt{1 - (1 - m)\sin^2\psi}\bigg). \tag{C13}$$

At $y \longrightarrow \infty$, the two first terms transform to the complete integrals with minus sign. The last term in (C13) diverges in the same way as the upper bound in (C7), so we can get rid of them both. Collecting (C7)–(C13), we come to the following formula for the potential:

$$\begin{aligned}\pi\alpha' V &= \frac{1}{a_c} + \sqrt{\frac{1}{a^2} + \xi_m^2}\mathrm{Re}[iK(m) - E(1 - m) - iE(m)],\\ &= \frac{1}{a_c} + \sqrt{\frac{1}{a^2} + \xi_m^2}\mathrm{Re}[iK(m) - \tilde{E}(m)],\end{aligned} \tag{C14}$$

where we also explicitly used only a real part of the expression as was done for L in (C5) and the defined common shorthand notation,

$$\tilde{E}(m) = E(1 - m) + iE(m). \tag{C15}$$

Similarly, starting from (44), one can obtain the second form of the potential,

$$\pi\alpha' V = \frac{1}{a_c} - \frac{\mathcal{C}L}{2} + \frac{\xi_m \mathcal{C}}{n}\mathrm{Re}[\tilde{K}(m) - n\tilde{\Pi}(n, m) - \tilde{E}(m)], \tag{C16}$$

where

$$\tilde{K}(m) = mK(1 - m) + iK(m). \tag{C17}$$

[1] D. N. Voskresensky and N. Yu. Anisimov, Properties of a pion condensate in a magnetic field, Zh. Eksp. Teor. Fiz. **78**, 2845 (1980) [Sov. Phys. JETP **51**, 13 (1980)], https://inspirehep.net/literature/159140.

[2] V. Skokov, A. Y. Illarionov, and V. D. Toneev, Estimate of the magnetic field strength in heavy-ion collisions, Int. J. Mod. Phys. A **24**, 5925 (2009).

[3] Adam Bzdak and Vladimir Skokov, Event-by-event fluctuations of magnetic and electric fields in heavy ion collisions, Phys. Lett. B **710**, 171 (2012).

[4] Wei-Tian Deng and Xu-Guang Huang, Event-by-event generation of electromagnetic fields in heavy-ion collisions, Phys. Rev. C **85**, 044907 (2012).

[5] John Bloczynski, Xu-Guang Huang, Xilin Zhang, and Jinfeng Liao, Azimuthally fluctuating magnetic field and its impacts on observables in heavy-ion collisions, Phys. Lett. B **718**, 1529 (2013).

[6] Umut Gursoy, Dmitri Kharzeev, and Krishna Rajagopal, Magnetohydrodynamics, charged currents and directed flow in heavy ion collisions, Phys. Rev. C **89**, 054905 (2014).

[7] Gabriele Inghirami, Luca Del Zanna, Andrea Beraudo, Mohsen Haddadi Moghaddam, Francesco Becattini, and Marcus Bleicher, Numerical magneto-hydrodynamics for relativistic nuclear collisions, Eur. Phys. J. C **76**, 659 (2016).

[8] V. Toneev, O. Rogachevsky, and V. Voronyuk, Evidence for creation of strong electromagnetic fields in relativistic heavy-ion collisions, Eur. Phys. J. A **52**, 264 (2016).

[9] Umut Gürsoy, Dmitri Kharzeev, Eric Marcus, Krishna Rajagopal, and Chun Shen, Charge-dependent flow induced by magnetic and electric fields in heavy ion collisions, Phys. Rev. C **98**, 055201 (2018).

[10] Bogdan V. Galilo and Sergei N. Nedelko, Impact of the strong electromagnetic field on the QCD effective potential for homogeneous Abelian gluon field configurations, Phys. Rev. D **84**, 094017 (2011).

[11] G. S. Bali, F. Bruckmann, G. Endrodi, Z. Fodor, S. D. Katz, and A. Schafer, QCD quark condensate in external magnetic fields, Phys. Rev. D **86**, 071502 (2012).

[12] Alejandro Ayala, M. Loewe, Ana Julia Mizher, and R. Zamora, Inverse magnetic catalysis for the chiral transition induced by thermo-magnetic effects on the coupling constant, Phys. Rev. D **90**, 036001 (2014).

[13] Niklas Mueller and Jan M. Pawlowski, Magnetic catalysis and inverse magnetic catalysis in QCD, Phys. Rev. D **91**, 116010 (2015).

[14] Shijun Mao, Inverse magnetic catalysis in Nambu–Jona-Lasinio model beyond mean field, Phys. Lett. B **758**, 195 (2016).

[15] R. L. S. Farias, V. S. Timoteo, S. S. Avancini, M. B. Pinto, and G. Krein, Thermo-magnetic effects in quark matter: Nambu–Jona-Lasinio model constrained by lattice QCD, Eur. Phys. J. A **53**, 101 (2017).

[16] V. V. Braguta, M. N. Chernodub, A. Yu Kotov, A. V. Molochkov, and A. A. Nikolaev, Finite-density QCD

transition in a magnetic background field, Phys. Rev. D **100**, 114503 (2019).

[17] Kenji Fukushima, Dmitri E. Kharzeev, and Harmen J. Warringa, The chiral magnetic effect, Phys. Rev. D **78**, 074033 (2008).

[18] A. V. Sadofyev, V. I. Shevchenko, and V. I. Zakharov, Notes on chiral hydrodynamics within effective theory approach, Phys. Rev. D **83**, 105025 (2011).

[19] V. D. Toneev, V. P. Konchakovski, V. Voronyuk, E. L. Bratkovskaya, and W. Cassing, Event-by-event background in estimates of the chiral magnetic effect, Phys. Rev. C **86**, 064907 (2012).

[20] Dmitri E. Kharzeev, The chiral magnetic effect and anomaly-induced transport, Prog. Part. Nucl. Phys. **75**, 133 (2014).

[21] Francesco Becattini, Iurii Karpenko, Michael Annan Lisa, Isaac Upsal, and Sergei A. Voloshin, Global hyperon polarization at local thermodynamic equilibrium with vorticity, magnetic field, and feed-down, Phys. Rev. C **95**, 054902 (2017).

[22] Yu Guo, Shuzhe Shi, Shengqin Feng, and Jinfeng Liao, Magnetic field induced polarization difference between hyperons and anti-hyperons, Phys. Lett. B **798**, 134929 (2019).

[23] Yu-Chen Liu and Xu-Guang Huang, Spin polarization formula for Dirac fermions at local equilibrium, Sci. China Phys. Mech. Astron. **65**, 272011 (2022).

[24] Kun Xu, Fan Lin, Anping Huang, and Mei Huang, $\Lambda/\bar{\Lambda}$ polarization and splitting induced by rotation and magnetic field, Phys. Rev. D **106**, L071502 (2022).

[25] Matteo Buzzegoli, Spin polarization induced by magnetic field and the relativistic Barnett effect, Nucl. Phys. **A1036**, 122674 (2023).

[26] Zhiwei Liu, Yunfan Bai, Shiqi Zheng, Anping Huang, and Baoyi Chen, Exploring spin polarization of heavy quarks in magnetic fields and hot medium, Phys. Rev. C **110**, 034910 (2024).

[27] Hidetoshi Taya, Toru Nishimura, and Akira Ohnishi, Estimation of electric field in intermediate-energy heavy-ion collisions, Phys. Rev. C **110**, 014901 (2024).

[28] Julian S. Schwinger, On gauge invariance and vacuum polarization, Phys. Rev. **82**, 664 (1951).

[29] Gerhard Baur, Kai Hencken, and Dirk Trautmann, Electron-positron pair production in relativistic heavy ion collisions, Phys. Rep. **453**, 1 (2007).

[30] Francois Gelis and Naoto Tanji, Schwinger mechanism revisited, Prog. Part. Nucl. Phys. **87**, 1 (2016).

[31] B. I. Abelev *et al.*, Global polarization measurement in Au + Au collisions, Phys. Rev. C **76**, 024915 (2007); **95**, 039906(E) (2017).

[32] L. Adamczyk *et al.*, Global Λ hyperon polarization in nuclear collisions: Evidence for the most vortical fluid, Nature (London) **548**, 62 (2017).

[33] J. Adam *et al.*, Global polarization of Ξ and Ω hyperons in Au + Au collisions at $\sqrt{s_{NN}} = 200$ GeV, Phys. Rev. Lett. **126**, 162301 (2021); **131**, 089901(E) (2023).

[34] R. Abou Yassine *et al.*, Measurement of global polarization of Λ hyperons in few-GeV heavy-ion collisions, Phys. Lett. B **835**, 137506 (2022).

[35] Apostolos D. Panagiotou, Λ^0 nonpolarization: Possible signature of quark matter, Phys. Rev. C **33**, 1999 (1986).

[36] J. W. Harris, A. Sandoval, R. Stock, H. Stroebele, R. E. Renfordt, J. V. Geaga, H. G. Pugh, L. S. Schroeder, K. L. Wolf, and A. Dacal, Λ production near threshold in central nucleus-nucleus collisions, Phys. Rev. Lett. **47**, 229 (1981).

[37] M. Anikina *et al.*, Characteristics of Λ and K^0 particles produced in central nucleus-nucleus collisions at a 4.5 GeV/c momentum per incident nucleon, Z. Phys. C **25**, 1 (1984).

[38] Jian-Hua Gao, Zuo-Tang Liang, Shi Pu, Qun Wang, and Xin-Nian Wang, Chiral anomaly and local polarization effect from the quantum kinetic approach, Phys. Rev. Lett. **109**, 232301 (2012).

[39] F. Becattini, V. Chandra, L. Del Zanna, and E. Grossi, Relativistic distribution function for particles with spin at local thermodynamical equilibrium, Ann. Phys. (Amsterdam) **338**, 32 (2013).

[40] Alexander Sorin and Oleg Teryaev, Axial anomaly and energy dependence of hyperon polarization in Heavy-Ion Collisions, Phys. Rev. C **95**, 011902 (2017).

[41] Oleg V. Teryaev and Valentin I. Zakharov, From the chiral vortical effect to polarization of baryons: A model, Phys. Rev. D **96**, 096023 (2017).

[42] L. P. Csernai, J. I. Kapusta, and T. Welle, Λ and $\bar{\Lambda}$ spin interaction with meson fields generated by the baryon current in high energy nuclear collisions, Phys. Rev. C **99**, 021901 (2019).

[43] F. Becattini, M. Buzzegoli, and A. Palermo, Spin-thermal shear coupling in a relativistic fluid, Phys. Lett. B **820**, 136519 (2021).

[44] Shuai Y. F. Liu and Yi Yin, Spin polarization induced by the hydrodynamic gradients, J. High Energy Phys. 07 (2021) 188.

[45] Cong Yi, Shi Pu, and Di-Lun Yang, Reexamination of local spin polarization beyond global equilibrium in relativistic heavy ion collisions, Phys. Rev. C **104**, 064901 (2021).

[46] Shuai Y. F. Liu and Yi Yin, Spin Hall effect in heavy-ion collisions, Phys. Rev. D **104**, 054043 (2021).

[47] Shu Lin and Ziyue Wang, Shear induced polarization: Collisional contributions, J. High Energy Phys. 12 (2022) 030.

[48] F. Becattini, L. Csernai, and D. J. Wang, Λ polarization in peripheral heavy ion collisions, Phys. Rev. C **88**, 034905 (2013); **93**, 069901(E) (2016).

[49] F. Becattini, G. Inghirami, V. Rolando, A. Beraudo, L. Del Zanna, A. De Pace, M. Nardi, G. Pagliara, and V. Chandra, A study of vorticity formation in high energy nuclear collisions, Eur. Phys. J. C **75**, 406 (2015); **78**, 354(E) (2018).

[50] F. Becattini, F. Piccinini, and J. Rizzo, Angular momentum conservation in heavy ion collisions at very high energy, Phys. Rev. C **77**, 024906 (2008).

[51] Jian-Hua Gao, Shou-Wan Chen, Wei-Tian Deng, Zuo-Tang Liang, Qun Wang, and Xin-Nian Wang, Global quark polarization in non-central A + A collisions, Phys. Rev. C **77**, 044902 (2008).

[52] Yin Jiang, Zi-Wei Lin, and Jinfeng Liao, Rotating quark-gluon plasma in relativistic heavy ion collisions, Phys. Rev. C **94**, 044910 (2016); **95**, 049904(E) (2017).

[53] Nils Sass, Marco Müller, Oscar Garcia-Montero, and Hannah Elfner, Global angular momentum generation in heavy-ion reactions within a hadronic transport approach, Phys. Rev. C **108**, 044903 (2023).

[54] N. S. Tsegelnik, E. E. Kolomeitsev, and V. Voronyuk, Helicity and vorticity in heavy-ion collisions at energies available at the JINR Nuclotron-based Ion Collider facility, Phys. Rev. C **107**, 034906 (2023).

[55] Oleg Teryaev and Rahim Usubov, Vorticity and hydrodynamic helicity in heavy-ion collisions in the hadron-string dynamics model, Phys. Rev. C **92**, 014906 (2015).

[56] Mircea Baznat, Konstantin Gudima, Alexander Sorin, and Oleg Teryaev, Femto-vortex sheets and hyperon polarization in heavy-ion collisions, Phys. Rev. C **93**, 031902 (2016).

[57] Wei-Tian Deng and Xu-Guang Huang, Vorticity in heavy-ion collisions, Phys. Rev. C **93**, 064907 (2016).

[58] Yu. B. Ivanov and A. A. Soldatov, Vorticity in heavy-ion collisions at the JINR Nuclotron-based Ion Collider fAcility, Phys. Rev. C **95**, 054915 (2017).

[59] Xiao-Liang Xia, Hui Li, Ze-Bo Tang, and Qun Wang, Probing vorticity structure in heavy-ion collisions by local Λ polarization, Phys. Rev. C **98**, 024905 (2018).

[60] E. E. Kolomeitsev, V. D. Toneev, and V. Voronyuk, Vorticity and hyperon polarization at energies available at JINR Nuclotron-based Ion Collider fAcility, Phys. Rev. C **97**, 064902 (2018).

[61] Xian-Gai Deng, Xu-Guang Huang, Yu-Gang Ma, and Song Zhang, Vorticity in low-energy heavy-ion collisions, Phys. Rev. C **101**, 064908 (2020).

[62] H. Petersen, The fastest-rotating fluid, Nature (London) **548**, 34 (2017).

[63] G. Yu. Prokhorov, D. A. Shohonov, O. V. Teryaev, N. S. Tsegelnik, and V. I. Zakharov, Modeling of acceleration in heavy-ion collisions: Occurrence of temperature below the Unruh temperature, Phys. Rev. C **112**, 064907 (2025).

[64] W. G. Unruh, Second quantization in the Kerr metric, Phys. Rev. D **10**, 3194 (1974).

[65] A. Vilenkin, Macroscopic parity violating effects: neutrino fluxes from rotating black holes and in rotating thermal radiation, Phys. Rev. D **20**, 1807 (1979).

[66] John R. Letaw and Jonathan D. Pfautsch, The quantized scalar field in rotating coordinates, Phys. Rev. D **22**, 1345 (1980).

[67] Bala R. Iyer, Dirac field theory in rotating coordinates, Phys. Rev. D **26**, 1900 (1982).

[68] Paul C. W. Davies, Tevian Dray, and Corinne A. Manogue, The rotating quantum vacuum, Phys. Rev. D **53**, 4382 (1996).

[69] Gavin Duffy and Adrian C. Ottewill, The rotating quantum thermal distribution, Phys. Rev. D **67**, 044002 (2003).

[70] Uwe R. Fischer and Gordon Baym, Vortex states of rapidly rotating dilute Bose-Einstein condensates, Phys. Rev. Lett. **90**, 140402 (2003).

[71] Arata Yamamoto and Yuji Hirono, Lattice QCD in rotating frames, Phys. Rev. Lett. **111**, 081601 (2013).

[72] Victor E. Ambruş and Elizabeth Winstanley, Rotating quantum states, Phys. Lett. B **734**, 296 (2014).

[73] Shu Ebihara, Kenji Fukushima, and Kazuya Mameda, Boundary effects and gapped dispersion in rotating fermionic matter, Phys. Lett. B **764**, 94 (2017).

[74] Yin Jiang and Jinfeng Liao, Pairing phase transitions of matter under rotation, Phys. Rev. Lett. **117**, 192302 (2016).

[75] M. N. Chernodub and Shinya Gongyo, Interacting fermions in rotation: Chiral symmetry restoration, moment of inertia and thermodynamics, J. High Energy Phys. 01 (2017) 136.

[76] Xinyang Wang, Minghua Wei, Zhibin Li, and Mei Huang, Quark matter under rotation in the NJL model with vector interaction, Phys. Rev. D **99**, 016018 (2019).

[77] Hui Zhang, Defu Hou, and Jinfeng Liao, Mesonic condensation in isospin matter under rotation, Chin. Phys. C **44**, 111001 (2020).

[78] M. N. Chernodub, Inhomogeneous confining-deconfining phases in rotating plasmas, Phys. Rev. D **103**, 054027 (2021).

[79] Yuki Fujimoto, Kenji Fukushima, and Yoshimasa Hidaka, Deconfining phase boundary of rapidly rotating hot and dense matter and analysis of moment of inertia, Phys. Lett. B **816**, 136184 (2021).

[80] Shi Chen, Kenji Fukushima, and Yusuke Shimada, Perturbative confinement in thermal Yang-Mills theories induced by imaginary angular velocity, Phys. Rev. Lett. **129**, 242002 (2022).

[81] Hao-Lei Chen, Zhi-Bin Zhu, and Xu-Guang Huang, Quark-meson model under rotation: A functional renormalization group study, Phys. Rev. D **108**, 054006 (2023).

[82] Fei Sun, Kun Xu, and Mei Huang, Splitting of chiral and deconfinement phase transitions induced by rotation, Phys. Rev. D **108**, 096007 (2023).

[83] Victor E. Ambruş and Maxim N. Chernodub, Rigidly rotating scalar fields: Between real divergence and imaginary fractalization, Phys. Rev. D **108**, 085016 (2023).

[84] D. N. Voskresensky, Pion-sigma meson vortices in rotating systems, Phys. Rev. D **109**, 034030 (2024).

[85] Fei Sun, Jingdong Shao, Rui Wen, Kun Xu, and Mei Huang, Chiral phase transition and spin alignment of vector mesons in the polarized-Polyakov-loop Nambu–Jona-Lasinio model under rotation, Phys. Rev. D **109**, 116017 (2024).

[86] Lutz Kiefer, Ashutosh Dash, and Dirk H. Rischke, Magnetization by Rotation: Spin and Chiral Condensates in the NJL Model, Phys. Rev. D **113**, 094032 (2026).

[87] William G. Unruh and Nathan Weiss, Acceleration radiation in interacting field theories, Phys. Rev. D **29**, 1656 (1984).

[88] Tadafumi Ohsaku, Dynamical chiral symmetry breaking and its restoration for an accelerated observer, Phys. Lett. B **599**, 102 (2004).

[89] Jan Ivar Korsbakken and Jon Magne Leinaas, The Fulling-Unruh effect in general stationary accelerated frames, Phys. Rev. D **70**, 084016 (2004).

[90] D. Ebert and V. Ch. Zhukovsky, Restoration of dynamically broken chiral and color symmetries for an accelerated observer, Phys. Lett. B **645**, 267 (2007).

[91] P. Castorina and M. Finocchiaro, Symmetry restoration by acceleration, J. Mod. Phys. **3**, 1703 (2012).

[92] Shingo Takeuchi, Bose–Einstein condensation in the Rindler space, Phys. Lett. B **750**, 209 (2015).

[93] Sanjin Benic and Kenji Fukushima, Unruh effect and condensate in and out of an accelerated vacuum, arXiv:1503.05790.
[94] F. Becattini, Thermodynamic equilibrium with acceleration and the Unruh effect, Phys. Rev. D **97**, 085013 (2018).
[95] George Y. Prokhorov, Oleg V. Teryaev, and Valentin I. Zakharov, Effects of rotation and acceleration in the axial current: Density operator vs Wigner function, J. High Energy Phys. 02 (2019) 146.
[96] G. Prokhorov, O. Teryaev, and V. Zakharov, Axial current in rotating and accelerating medium, Phys. Rev. D **98**, 071901 (2018).
[97] Fabio Scardigli, Massimo Blasone, Gaetano Luciano, and Roberto Casadio, Modified Unruh effect from generalized uncertainty principle, Eur. Phys. J. C **78**, 728 (2018).
[98] George Y. Prokhorov, Oleg V. Teryaev, and Valentin I. Zakharov, Unruh effect for fermions from the Zubarev density operator, Phys. Rev. D **99**, 071901 (2019).
[99] Andrea Palermo, Matteo Buzzegoli, and Francesco Becattini, Exact equilibrium distributions in statistical quantum field theory with rotation and acceleration: Dirac field, J. High Energy Phys. 10 (2021) 077.
[100] E. T. Akhmedov, K. V. Bazarov, and D. V. Diakonov, Quantum fields in the future Rindler wedge, Phys. Rev. D **104**, 085008 (2021).
[101] M. N. Chernodub, V. A. Goy, A. V. Molochkov, D. V. Stepanov, and A. S, Pochinok, Extreme softening of QCD phase transition under weak acceleration: First-principles Monte Carlo results for gluon plasma, Phys. Rev. Lett. **134**, 111904 (2025).
[102] Maxim N. Chernodub, Acceleration as refrigeration: Acceleration-induced spontaneous symmetry breaking in thermal medium, arXiv:2501.16129.
[103] M. Bordag and D. N. Voskresensky, Charged scalar bosons under rotation and acceleration, Phys. Part. Nucl. Lett. **23**, 139 (2026).
[104] G. Yu. Prokhorov, Entanglement viscosity: From unitarity to irreversibility in accelerated frames, arXiv:2601.02083.
[105] Hao-Lei Chen, Kenji Fukushima, Xu-Guang Huang, and Kazuya Mameda, Analogy between rotation and density for Dirac fermions in a magnetic field, Phys. Rev. D **93**, 104052 (2016).
[106] Yizhuang Liu and Ismail Zahed, Pion condensation by rotation in a magnetic field, Phys. Rev. Lett. **120**, 032001 (2018).
[107] Yizhuang Liu and Ismail Zahed, Rotating Dirac fermions in a magnetic field in $1+2$ and $1+3$ dimensions, Phys. Rev. D **98**, 014017 (2018).
[108] Kenji Fukushima, Extreme matter in electromagnetic fields and rotation, Prog. Part. Nucl. Phys. **107**, 167 (2019).
[109] N. Sadooghi, S. M. A. Tabatabaee Mehr, and F. Taghinavaz, Inverse magnetorotational catalysis and the phase diagram of a rotating hot and magnetized quark matter, Phys. Rev. D **104**, 116022 (2021).
[110] D. N. Voskresensky, Pion condensation at rotation in magnetic field, electric, and scalar potential wells, Phys. Rev. D **111**, 036022 (2025).
[111] V. V. Braguta, A. Yu. Kotov, D. D. Kuznedelev, and A. A. Roenko, Study of the confinement/deconfinement phase transition in rotating lattice SU(3) gluodynamics, JETP Lett. **112**, 6 (2020).
[112] V. V. Braguta, A. Yu. Kotov, D. D. Kuznedelev, and A. A. Roenko, Influence of relativistic rotation on the confinement-deconfinement transition in gluodynamics, Phys. Rev. D **103**, 094515 (2021).
[113] Victor Braguta, A. Yu. Kotov, Denis Kuznedelev, and Artem Roenko, Lattice study of the confinement/deconfinement transition in rotating gluodynamics, Proc. Sci. LATTICE2021 (**2022**) 125.
[114] V. V. Braguta, Andrey Kotov, Artem Roenko, and Dmitry Sychev, Thermal phase transitions in rotating QCD with dynamical quarks, Proc. Sci. LATTICE2022 (**2023**) 190.
[115] V. V. Braguta, M. N. Chernodub, I. E. Kudrov, A. A. Roenko, and D. A. Sychev, Influence of relativistic rotation on QCD properties, Phys. At. Nucl. **86**, 1249 (2023).
[116] Ji-Chong Yang and Xu-Guang Huang, QCD on rotating lattice with staggered fermions, arXiv:2307.05755.
[117] M. N. Chernodub, V. A. Goy, and A. V. Molochkov, Inhomogeneity of a rotating gluon plasma and the Tolman-Ehrenfest law in imaginary time: Lattice results for fast imaginary rotation, Phys. Rev. D **107**, 114502 (2023).
[118] V. V. Braguta, I. E. Kudrov, A. A. Roenko, D. A. Sychev, and M. N. Chernodub, Lattice study of the equation of state of a rotating gluon plasma, JETP Lett. **117**, 639 (2023).
[119] Victor V. Braguta, Maxim N. Chernodub, Artem A. Roenko, and Dmitrii A. Sychev, Negative moment of inertia and rotational instability of gluon plasma, Phys. Lett. B **852**, 138604 (2024).
[120] Victor V. Braguta, Maxim N. Chernodub, Ilya E. Kudrov, Artem A. Roenko, and Dmitrii A. Sychev, Moment of inertia and supervortical temperature of gluon plasma, Proc. Sci. LATTICE2023 (**2024**) 181.
[121] Victor V. Braguta, Maxim N. Chernodub, Ilya E. Kudrov, Artem A. Roenko, and Dmitrii A. Sychev, Negative Barnett effect, negative moment of inertia of the gluon plasma, and thermal evaporation of the chromomagnetic condensate, Phys. Rev. D **110**, 014511 (2024).
[122] Victor V. Braguta, Maxim N. Chernodub, and Artem A. Roenko, New mixed inhomogeneous phase in vortical gluon plasma: First-principle results from rotating SU(3) lattice gauge theory, Phys. Lett. B **855**, 138783 (2024).
[123] V. Braguta, M. Chernodub, E. Eremeev, I. Kudrov, A. Roenko, and D. Sychev, On the angular momentum and free energy of rotating gluon plasma, arXiv:2512.04070.
[124] Juan Martin Maldacena, The large N limit of superconformal field theories and supergravity, Adv. Theor. Math. Phys. **2**, 231 (1998).
[125] Oliver DeWolfe, Steven S. Gubser, Christopher Rosen, and Derek Teaney, Heavy ions and string theory, Prog. Part. Nucl. Phys. **75**, 86 (2014).
[126] Jorge Casalderrey-Solana, Hong Liu, David Mateos, Krishna Rajagopal, and Urs Achim Wiedemann, *Gauge/String Duality, Hot QCD and Heavy Ion Collisions* (Cambridge University Press, Cambridge, England, 2014).
[127] I. Ya Aref'eva, Holographic approach to quark–gluon plasma in heavy ion collisions, Phys. Usp. **57**, 527 (2014).
[128] Juan Maldacena, Wilson loops in large N field theories, Phys. Rev. Lett. **80**, 4859 (1998).

[129] Soo-Jong Rey, Stefan Theisen, and Jung-Tay Yee, Wilson-Polyakov loop at finite temperature in large-n gauge theory and anti-de Sitter supergravity, Nucl. Phys. **B527**, 171 (1998).

[130] A Brandhuber, N Itzhaki, J Sonnenschein, and S Yankielowicz, Wilson loops in the large N limit at finite temperature, Phys. Lett. B **434**, 36 (1998).

[131] A. Brandhuber and K. Sfetsos, Wilson loops from multicenter and rotating branes, mass gaps and phase structure in gauge theories, Adv. Theor. Math. Phys. **3**, 851 (1999).

[132] Y. Kinar, E. Schreiber, and J. Sonnenschein, $Q\bar{Q}$ potential from strings in curved space-time—classical results, Nucl. Phys. **B566**, 103 (2000).

[133] Soo-Jong Rey and Jung-Tay Yee, Macroscopic strings as heavy quarks in large N gauge theory and anti-de Sitter supergravity, Eur. Phys. J. C **22**, 379 (2001).

[134] Henrique Boschi-Filho, Nelson R. F. Braga, and Cristine N. Ferreira, Heavy quark potential at finite temperature from gauge/string duality, Phys. Rev. D **74**, 086001 (2006).

[135] Hong Liu, Krishna Rajagopal, and Urs Achim Wiedemann, Wilson loops in heavy ion collisions and their calculation in AdS/CFT, J. High Energy Phys. 03 (2007) 066.

[136] C D White, The Cornell potential from general geometries in AdS/QCD, Phys. Lett. B **652**, 79 (2007).

[137] Dimitrios Giataganas, Probing strongly coupled anisotropic plasma, J. High Energy Phys. 07 (2012) 031.

[138] Dimitrios Giataganas and Nikos Irges, Flavor corrections in the static potential in holographic QCD, Phys. Rev. D **85**, 046001 (2012).

[139] Edward Witten, Anti-de Sitter space, thermal phase transition, and confinement in gauge theories, Adv. Theor. Math. Phys. **2**, 505 (1998).

[140] Bo Sundborg, The hagedorn transition, deconfinement and $N = 4$ SYM theory, Nucl. Phys. **B573**, 349 (2000).

[141] Marcus Spradlin and Anastasia Volovich, The one-loop partition function of $N = 4$ super-Yang–Mills theory on $\mathbb{R} \times S^3$, Nucl. Phys. **B711**, 199 (2005).

[142] Joseph Polchinski and Matthew J. Strassler, The String dual of a confining four-dimensional gauge theory, arXiv: hep-th/0003136.

[143] Y. M. Cho and Ishwaree P. Neupane, Anti-de Sitter black holes, thermal phase transition and holography in higher curvature gravity, Phys. Rev. D **66**, 024044 (2002).

[144] Ofer Aharony, Joseph Marsano, Shiraz Minwalla, Kyriakos Papadodimas, and Mark Van Raamsdonk, The hagedorn—deconfinement phase transition in weakly coupled large N gauge theories, Adv. Theor. Math. Phys. **8**, 603 (2004).

[145] Andreas Karch, Emanuel Katz, Dam T. Son, and Mikhail A. Stephanov, Linear confinement and AdS/QCD, Phys. Rev. D **74**, 015005 (2006).

[146] C. A. Ballon Bayona, Henrique Boschi-Filho, Nelson R. F. Braga, and Leopoldo A, Pando Zayas, On a holographic model for confinement/deconfinement, Phys. Rev. D **77**, 046002 (2008).

[147] U. Gursoy, E. Kiritsis, L. Mazzanti, and F. Nitti, Holography and thermodynamics of 5D dilaton-gravity, J. High Energy Phys. 05 (2009) 033.

[148] Donald Marolf, Mukund Rangamani, and Toby Wiseman, Holographic thermal field theory on curved spacetimes, Classical Quantum Gravity **31**, 063001 (2014).

[149] Stanley J. Brodsky, Guy F. de Teramond, Hans Gunter Dosch, and Joshua Erlich, Light-front holographic QCD and emerging confinement, Phys. Rep. **584**, 1 (2015).

[150] Troels Harmark and Matthias Wilhelm, Hagedorn temperature of AdS_5/CFT_4 via integrability, Phys. Rev. Lett. **120**, 071605 (2018).

[151] Sang-Jin Sin and Ismail Zahed, Holography of radiation and jet quenching, Phys. Lett. B **608**, 265 (2005).

[152] Christopher P. Herzog, Energy loss of heavy quarks from asymptotically AdS geometries, J. High Energy Phys. 09 (2006) 032.

[153] C. P. Herzog, A. Karch, P. Kovtun, C. Kozcaz, and L. G. Yaffe, Energy loss of a heavy quark moving through $N = 4$ supersymmetric Yang-Mills plasma, J. High Energy Phys. 07 (2006) 013.

[154] Steven S. Gubser, Drag force in AdS/CFT, Phys. Rev. D **74**, 126005 (2006).

[155] Hong Liu, Krishna Rajagopal, and Urs Achim Wiedemann, Calculating the jet quenching parameter from AdS/CFT, Phys. Rev. Lett. **97**, 182301 (2006).

[156] Mariano Chernicoff, Daniel Fernandez, David Mateos, and Diego Trancanelli, Jet quenching in a strongly coupled anisotropic plasma, J. High Energy Phys. 08 (2012) 041.

[157] Emil T. Akhmedov, A remark on the AdS/CFT correspondence and the renormalization group flow, Phys. Lett. B **442**, 152 (1998).

[158] Dam T. Son and Andrei O. Starinets, Minkowski space correlators in AdS/CFT correspondence: Recipe and applications, J. High Energy Phys. 09 (2002) 042.

[159] Joseph Polchinski and Matthew J. Strassler, Hard scattering and gauge/string duality, Phys. Rev. Lett. **88**, 031601 (2002).

[160] Henrique Boschi-Filho and Nelson R. F. Braga, Gauge/string duality and scalar glueball mass ratios, J. High Energy Phys. 05 (2003) 009.

[161] Henrique Boschi-Filho and Nelson R. F. Braga, QCD/string holographic mapping and glueball mass spectrum, Eur. Phys. J. C **32**, 529 (2004).

[162] P. Kovtun, Dan T. Son, and Andrei O. Starinets, Viscosity in strongly interacting quantum field theories from black hole physics, Phys. Rev. Lett. **94**, 111601 (2005).

[163] Jorge Casalderrey-Solana and Derek Teaney, Heavy quark diffusion in strongly coupled $N = 4$ Yang-Mills, Phys. Rev. D **74**, 085012 (2006).

[164] Hong Liu, Krishna Rajagopal, and Urs Achim Wiedemann, An AdS/CFT calculation of screening in a hot wind, Phys. Rev. Lett. **98**, 182301 (2007).

[165] Shinsei Ryu and Tadashi Takayanagi, Holographic derivation of entanglement entropy from AdS/CFT, Phys. Rev. Lett. **96**, 181602 (2006).

[166] Edward Shuryak, Sang-Jin Sin, and Ismail Zahed, A gravity dual of RHIC collisions, J. Korean Phys. Soc. **50**, 384 (2007).

[167] Daniel Grumiller and Paul Romatschke, On the collision of two shock waves in AdS_5, J. High Energy Phys. 08 (2008) 027.

[168] N. P. Bobev, H. Dimov, and R. C. Rashkov, Semiclassical strings in Lunin-Maldacena background, Bulg. J. Phys. **35**, 274 (2008), https://inspirehep.net/literature/684416.
[169] Steven S. Gubser, Silviu S. Pufu, and Amos Yarom, Off-center collisions in AdS_5 with applications to multiplicity estimates in heavy-ion collisions, J. High Energy Phys. 11 (2009) 050.
[170] E. T. Akhmedov, I. B. Gahramanov, and E. T. Musaev, Hints on integrability in the Wilsonian/holographic renormalization group, JETP Lett. **93**, 545 (2011).
[171] David Mateos and Diego Trancanelli, The anisotropic $N = 4$ super Yang-Mills plasma and its instabilities, Phys. Rev. Lett. **107**, 101601 (2011).
[172] Michael Strickland, Thermalization and isotropization in heavy-ion collisions, Pramana **84**, 671 (2015).
[173] Dimitrios Giataganas, Umut Gürsoy, and Juan F. Pedraza, Strongly-coupled anisotropic gauge theories and holography, Phys. Rev. Lett. **121**, 121601 (2018).
[174] Chong-Sun Chu and Dimitrios Giataganas, c-theorem for anisotropic RG flows from holographic entanglement entropy, Phys. Rev. D **101**, 046007 (2020).
[175] H. Dimov, R. C. Rashkov, and T. Vetsov, Thermodynamic information geometry and complexity growth of a warped AdS black hole and the warped AdS_3/CFT_2 correspondence, Phys. Rev. D **99**, 126007 (2019).
[176] Dimitrios Giataganas, Velocity laws for bound states in asymptotically AdS geometries, Fortschr. Phys. **71**, 2300030 (2023).
[177] V. Avramov, H. Dimov, M. Radomirov, R. C. Rashkov, and T. Vetsov, On thermodynamic stability of black holes. Part I: Classical stability, Eur. Phys. J. C **84**, 281 (2024).
[178] Ksenia Arkhipova, Lev Astrakhantsev, Nihat Sadik Deger, Anastasia A. Golubtsova, Kirill Gubarev, and Edvard T. Musaev, Holographic RG flows and boundary conditions in a 3D gauged supergravity, Eur. Phys. J. C **84**, 560 (2024).
[179] Lev Astrakhantsev, Anastasia A. Golubtsova, and Mikhail A. Podoinitsyn, Zoo of flows in a 3d gauged supergravity with periodic potential, 2025.
[180] S. W. Hawking and H. S. Reall, Charged and rotating AdS black holes and their CFT duals, Phys. Rev. D **61**, 024014 (2000).
[181] Elena Caceres and Alberto Guijosa, Drag force in charged $N = 4$ SYM plasma, J. High Energy Phys. 11 (2006) 077.
[182] Eric D'Hoker and Per Kraus, Charged magnetic brane solutions in AdS_5 and the fate of the third law of thermodynamics, J. High Energy Phys. 03 (2010) 095.
[183] Alfonso Ballon-Bayona, Holographic deconfinement transition in the presence of a magnetic field, J. High Energy Phys. 11 (2013) 168.
[184] David Dudal and Thomas G. Mertens, Melting of charmonium in a magnetic field from an effective AdS/QCD model, Phys. Rev. D **91**, 086002 (2015).
[185] Nick Evans, Carlisson Miller, and Marc Scott, Inverse magnetic catalysis in bottom-up holographic QCD, Phys. Rev. D **94**, 074034 (2016).
[186] Danning Li, Mei Huang, Yi Yang, and Pei-Hung Yuan, Inverse magnetic catalysis in the soft-wall model of AdS/QCD, J. High Energy Phys. 02 (2017) 030.
[187] Irina Aref'eva and Kristina Rannu, Holographic anisotropic background with confinement-deconfinement phase transition, J. High Energy Phys. 05 (2018) 206.
[188] Nelson R. F. Braga and Luiz F. Ferreira, Heavy meson dissociation in a plasma with magnetic fields, Phys. Lett. B **783**, 186 (2018).
[189] David Dudal and Thomas G. Mertens, Holographic estimate of heavy quark diffusion in a magnetic field, Phys. Rev. D **97**, 054035 (2018).
[190] Wenxing Cheng and Zi-qiang Zhang, Heavy quark potential in STU and AdS_5–Reissner–Nordstrom backgrounds, Eur. Phys. J. C **85**, 774 (2025).
[191] S. W. Hawking, C. J. Hunter, and Marika Taylor, Rotation and the AdS/CFT correspondence, Phys. Rev. D **59**, 064005 (1999).
[192] G. W. Gibbons, M. J. Perry, and C. N. Pope, The First law of thermodynamics for Kerr-anti-de Sitter black holes, Classical Quantum Gravity **22**, 1503 (2005).
[193] Sayantani Bhattacharyya, Subhaneil Lahiri, R. Loganayagam, and Shiraz Minwalla, Large rotating AdS black holes from fluid mechanics, J. High Energy Phys. 09 (2008) 054.
[194] A. Nata Atmaja and K. Schalm, Anisotropic drag force from 4D Kerr-AdS black holes, J. High Energy Phys. 04 (2011) 070.
[195] Brett Mcinnes, Applied holography of the AdS_5–Kerr space–time, Int. J. Mod. Phys. A **34**, 1950138 (2019).
[196] Irina Ya. Aref'eva, Anastasia A. Golubtsova, and Eric Gourgoulhon, Holographic drag force in 5d Kerr-AdS black hole, J. High Energy Phys. 04 (2021) 169.
[197] Anastasia A. Golubtsova, Eric Gourgoulhon, and Marina K. Usova, Heavy quarks in rotating plasma via holography, Nucl. Phys. **B979**, 115786 (2022).
[198] Nelson R. F. Braga, Luiz F. Faulhaber, and Octavio C. Junqueira, Confinement-deconfinement temperature for a rotating quark-gluon plasma, Phys. Rev. D **105**, 106003 (2022).
[199] Yidian Chen, Danning Li, and Mei Huang, Inhomogeneous chiral condensation under rotation in the holographic QCD, Phys. Rev. D **106**, 106002 (2022).
[200] Brett McInnes, Why is black hole entropy affected by rotation?, J. High Energy Phys. 02 (2023) 072.
[201] Gopal Yadav, Deconfinement temperature of rotating QGP at intermediate coupling from M-theory, Phys. Lett. B **841**, 137925 (2023).
[202] Nelson R. F. Braga, Luiz F. Ferreira, and Octavio C. Junqueira, Configuration entropy of a rotating quark-gluon plasma from holography, Phys. Lett. B **847**, 138265 (2023).
[203] Nelson R. F. Braga and Yan F. Ferreira, Bottomonium dissociation in a rotating plasma, Phys. Rev. D **108**, 094017 (2023).
[204] Anastasia Golubtsova and Nikita Tsegelnik, Probing the holographic model of $\mathcal{N} = 4$ sym rotating quark-gluon plasma, Phys. Rev. D **107**, 106017 (2023).
[205] Jun-Xia Chen and De-Fu Hou, Heavy quark potential and jet quenching parameter in a rotating D-instanton background, Eur. Phys. J. C **84**, 447 (2024).

[206] Jun-Xia Chen, De-Fu Hou, and Hai-Cang Ren, Drag force and heavy quark potential in a rotating background, J. High Energy Phys. 03 (2024) 171.
[207] Nelson R. F. Braga and Octavio C. Junqueira, Inhomogeneity of a rotating quark-gluon plasma from holography, Phys. Lett. B **848**, 138330 (2024).
[208] Yi-ze Cai and Zi-qiang Zhang, Holographic Schwinger effect in spinning black hole backgrounds, Chin. Phys. C **48**, 015102 (2024).
[209] Jun-Xia Chen, Sheng Wang, Defu Hou, and Hai-Cang Ren, String tension and Polyakov loop in a rotating background, Phys. Rev. D **111**, 026020 (2025).
[210] Luiz F. Ferreira, Dispersion relations and pole-skipping in a holographic charmonium model with rotating plasma, Phys. Rev. D **112**, 074043 (2025).
[211] Zhou-Run Zhu, Sheng Wang, Man-Li Tian, and Defu Hou, Running coupling constant and jet quenching parameter in the spinning background from holography, Phys. Rev. D **113**, 066014 (2026).
[212] Nelson R. F. Braga and Octavio C. Junqueira, Holographic QCD phase diagram for a rotating plasma in the Hawking-Page approach, Phys. Lett. B **868**, 139669 (2025).
[213] Brett McInnes, Angular momentum in QGP holography, Nucl. Phys. **B887**, 246 (2014).
[214] Brett McInnes, A rotation/magnetism analogy for the quark–gluon plasma, Nucl. Phys. B **911**, 173 (2016).
[215] Xun Chen, Lin Zhang, Danning Li, Defu Hou, and Mei Huang, Gluodynamics and deconfinement phase transition under rotation from holography, J. High Energy Phys. 07 (2021) 132.
[216] Defu Hou, Mahdi Atashi, Kazem Bitaghsir Fadafan, and Zi-qiang Zhang, Holographic energy loss of a rotating heavy quark at finite chemical potential, Phys. Lett. B **817**, 136279 (2021).
[217] Luis A. H. Mamani, Defu Hou, and Nelson R. F. Braga, Melting of heavy vector mesons and quasinormal modes in a finite density plasma from holography, Phys. Rev. D **105**, 126020 (2022).
[218] Yan-Qing Zhao, Song He, Defu Hou, Li Li, and Zhibin Li, Phase diagram of holographic thermal dense QCD matter with rotation, J. High Energy Phys. 04 (2023) 115.
[219] Jia-Hao Wang and Sheng-Qin Feng, Rotation effect on the deconfinement phase transition in holographic QCD, Phys. Rev. D **109**, 066019 (2024).
[220] Yidian Chen, Xun Chen, Danning Li, and Mei Huang, Deconfinement and chiral restoration phase transition under rotation from holography in an anisotropic gravitational background, Phys. Rev. D **111**, 046006 (2025).
[221] Hiwa A. Ahmed, Yidian Chen, and Mei Huang, Gluon polarization contribution to the spin alignment of vector mesons from holography, Phys. Rev. D **111**, 086006 (2025).
[222] Stanley Deser and Orit Levin, Accelerated detectors and temperature in (anti)-de Sitter spaces, Classical Quantum Gravity **14**, L163 (1997).
[223] Alex Hamilton, Daniel N. Kabat, Gilad Lifschytz, and David A. Lowe, Holographic representation of local bulk operators, Phys. Rev. D **74**, 066009 (2006).
[224] J. Podolsky and J. B. Griffiths, Accelerating Kerr-Newman black holes in (anti-)de Sitter space-time, Phys. Rev. D **73**, 044018 (2006).
[225] Mariano Chernicoff and Alberto Guijosa, Acceleration, energy loss and screening in strongly-coupled gauge theories, J. High Energy Phys. 06 (2008) 005.
[226] J. G. Russo and P. K. Townsend, Accelerating branes and brane temperature, Classical Quantum Gravity **25**, 175017 (2008).
[227] Kazuo Ghoroku, Masafumi Ishihara, Kouki Kubo, and Tomoki Taminato, Accelerated quark and holography for confining gauge theory, Phys. Rev. D **83**, 024020 (2011).
[228] Takayuki Hirayama, Pei-Wen Kao, Shoichi Kawamoto, and Feng-Li Lin, Unruh effect and holography, Nucl. Phys. **B844**, 1 (2011).
[229] Mariano Chernicoff and Angel Paredes, Accelerated detectors and worldsheet horizons in AdS/CFT, J. High Energy Phys. 03 (2011) 063.
[230] Bartlomiej Czech, Joanna L. Karczmarek, Fernando Nogueira, and Mark Van Raamsdonk, Rindler quantum gravity, Classical Quantum Gravity **29**, 235025 (2012).
[231] Maulik Parikh, Prasant Samantray, and Erik Verlinde, Rotating Rindler-AdS space, Phys. Rev. D **86**, 024005 (2012).
[232] Reza Fareghbal and Ali Naseh, Rindler/contracted-CFT correspondence, J. High Energy Phys. 06 (2014) 134.
[233] Ahmed Almheiri, Xi Dong, and Daniel Harlow, Bulk locality and quantum error correction in AdS/CFT, J. High Energy Phys. 04 (2015) 163.
[234] Marco Astorino, CFT duals for accelerating black holes, Phys. Lett. B **760**, 393 (2016).
[235] Michael Appels, Ruth Gregory, and David Kubiznak, Thermodynamics of accelerating black holes, Phys. Rev. Lett. **117**, 131303 (2016).
[236] Maulik Parikh and Prasant Samantray, Rindler-AdS/CFT, J. High Energy Phys. 10 (2018) 129.
[237] Andrés Anabalón, Finnian Gray, Ruth Gregory, David Kubizňák, and Robert B. Mann, Thermodynamics of charged, rotating, and accelerating black holes, J. High Energy Phys. 04 (2019) 096.
[238] Andrés Anabalón, Michael Appels, Ruth Gregory, David Kubizňák, Robert B. Mann, and Alï Ovgün, Holographic thermodynamics of accelerating black holes, Phys. Rev. D **98**, 104038 (2018).
[239] Ruth Gregory and Andrew Scoins, Accelerating black hole chemistry, Phys. Lett. B **796**, 191 (2019).
[240] Pietro Ferrero, Jerome P. Gauntlett, Juan Manuel Pérez Ipiña, Dario Martelli, and James Sparks, Accelerating black holes and spinning spindles, Phys. Rev. D **104**, 046007 (2021).
[241] Davide Cassani, Jerome P. Gauntlett, Dario Martelli, and James Sparks, Thermodynamics of accelerating and supersymmetric AdS_4 black holes, Phys. Rev. D **104**, 086005 (2021).
[242] Sotaro Sugishita and Seiji Terashima, Rindler bulk reconstruction and subregion duality in AdS/CFT, J. High Energy Phys. 11 (2022) 041.
[243] Jose Barrientos, Adolfo Cisterna, David Kubiznak, and Julio Oliva, Accelerated black holes beyond Maxwell's electrodynamics, Phys. Lett. B **834**, 137447 (2022).

[244] Di Wu, Topological classes of thermodynamics of the four-dimensional static accelerating black holes, Phys. Rev. D **108**, 084041 (2023).
[245] Xin-Xiang Ju, Wen-Bin Pan, Ya-Wen Sun, and Yuan-Tai Wang, Generalized Rindler Wedge and Holographic Observer Concordance, arXiv:2302.03340.
[246] Gabriel Arenas-Henriquez, Adolfo Cisterna, Felipe Diaz, and Ruth Gregory, Accelerating black holes in $2+1$ dimensions: Holography revisited, J. High Energy Phys. 09 (2023) 122.
[247] Xin-Xiang Ju, Bo-Hao Liu, Wen-Bin Pan, Ya-Wen Sun, and Yuan-Tai Wang, Squashed entanglement from generalized Rindler wedge, J. High Energy Phys. 09 (2025) 006.
[248] In fact, this is *the reduced Hamiltonian density*, but for brevity we will simply call it the Hamiltonian density. For details see Appendix A.
[249] G. W.Gibbons, M. J. Perry, and C. N. Pope, The first law of thermodynamics for Kerr−anti−de Sitterblack holes, Classical Quantum Gravity **22**, 1503 (2005).
[250] Spyros D. Avramis, Konstadinos Sfetsos, and Dimitrios Zoakos, On the velocity and chemical-potential dependence of the heavy-quark interaction in $N=4$ SYM plasmas, Phys. Rev. D **75**, 025009 (2007).
[251] Harald Dorn and Thanh Hai Ngo, On the internal space dependence of the static quark-antiquark potential in $N=4$ SYM plasma wind, Phys. Lett. B **654**, 41 (2007).
[252] Nadav Drukker and Valentina Forini, Generalized quark-antiquark potential at weak and strong coupling, J. High Energy Phys. 06 (2011) 131.
[253] Viktor Braguta, Vladimir Goy, Jayanta Dey, and Artem Roenko, Spatial confinement-deconfinement transition in accelerated gluodynamics within lattice simulation, Phys. Rev. D **113**, 094507 (2026).
[254] Victor V. Braguta, Vladimir A. Goy, Jayanta Dey, and Artem A. Roenko, Spatially inhomogeneous confinement-deconfinement phase transition in accelerated gluodynamics, in *42th International Symposium on Lattice Field Theory* (Tata Institute of Fundamental Research (TIFR), Mumbai, India, 2025).